Title: Structure and thermal history of the Wełnowiec dump, Poland : a municipal dump rehabilitated with coal waste

Author: Jolanta Pierwoła, Justyna Ciesielczuk, Magdalena Misz-Kennan, Monika Fabiańska, A. Bielińska, Ł. Kruszewski

Citation style Pierwoła Jolanta, Ciesielczuk Justyna, Misz-Kennan Magdalena, Fabiańska Monika, Bielińska A., Kruszewski Ł. (2018). Structure and thermal history of the Wełnowiec dump, Poland : a municipal dump rehabilitated with coal waste. "International Journal of Coal Geology" Vol. 197 (2018), s. 1-19. doi: 10.1016/j.coal.2018.08.001

International Journal of Coal Geology 197 (2018) 1–19

Contents lists available at ScienceDirect

International Journal of Coal Geology

journal homepage: www.elsevier.com/locate/coal

Structure and thermal history of the Wełnowiec dump, Poland: A municipal dump rehabilitated with coal waste

Pierwoła J.[a], Ciesielczuk J.[a,*], Misz-Kennan M.[a], Fabiańska M.J.[a], Bielińska A.[a], Kruszewski Ł.[b]

[a] Faculty of Earth Sciences, University of Silesia, 60 Będzińska St., PL-41-200 Sosnowiec, Poland
[b] Institute of Geological Sciences, Polish Academy of Sciences (ING PAN), 51/55 Twarda St., PL-00-818 Warsaw, Poland

ARTICLE INFO

Keywords:
Self-heating
Thermal zones
Coal wastes
Electrical resistivity tomography (ERT)
Conductivity profiling (FDEM)
Mineralogy
Geochemistry

ABSTRACT

The Wełnowiec municipal dump, Katowice, Poland, rehabilitated with coal waste, is self-heating and igniting. This paper presents a novel application of the use of electrical- and resistivity geophysical methods in the investigation of burning coal waste to help explain why the heating occurred. Geoelectrical methods allowed the internal structure of the dump to be revealed, and the municipal wastes and their rehabilitation cover containing coal waste to be differentiated. Instead of a planned 2.2-m-thick multi-barrier system, the cover consists of irregularly distributed material of varying thickness (< 1 to 8 m) and organic carbon content (> 5%). This caused the fire to arise 3–4 years after the coal waste deposition. In areas where the rehabilitation layer is < 3 m thick, a landslide enabled oxygen access, initiating self-heating. Changes in conductivity clearly identify sites of active burning where measured conductivity values are more than twice those for parts of the dump with no thermal activity. Field observations in particular, complemented to a degree by petrographic, mineralogical and geochemical data, enabled four types of heating zones to be distinguished, namely, (1) initial zones of fire overtaking new volumes of coal waste, (2) active zones with temperatures < 400–500 °C in exhalation vents, (3) overburned zones characterized by long-lasting high temperatures (800-900 °C) and (4) short-lived zones, ephemeral (< 1–2 months) with temperatures between 70 and 100 °C. The geophysical methods applied could not distinguish between these zones. The combined results strongly suggest that the use of coal waste as a remediation layer covering waste dumps should be prohibited. Coal waste which, by its nature, is too prone to unpredictable self-heating and self-ignition with the potential environmental consequences that follow.

1. Introduction

1.1. Self-heating in coal-waste dumps

During coal exploitation, associated claystones, mudstones, sandstones, carbonates, and conglomerates, etc., all contribute to the 0.3–0.7 tons of waste produced from every ton of coal mined in Poland (Skarżyńska, 1995). Much of this waste is deposited in dumps where oxidation of both organic- and mineral matter occurs. In some cases, self-heating leading to ignition and burning of the waste may occur, but only where three factors combine, namely, the presence of organic matter, access for air, and accumulation of heat within a dump (Brooks et al., 1988; Kaymakçi and Didari, 2002; Pone et al., 2007). Oxidation of sulphides, mostly pyrite, adds heat. After dumping, oxidation takes place and temperatures rise slowly without any external signs of the process. As temperatures reach 60–80 °C, the heat may either dissipate or suddenly start to rise rapidly to the point of ignition, i.e., ca 200 °C for hard coals (Sawicki, 2004; Sokol et al., 2005; Pone et al., 2007). The temperature of burning waste can exceed 1300 °C (Sawicki, 2004; Sokol et al., 2005). The thermal processes happening within a dump take place where access to air is limited, and commonly in the presence of water (rain); these are pyrolytic or/and hydropyrolytic processes (Fabiańska et al., 2013; Misz-Kennan and Fabiańska, 2011).

Factors that influence the self-heating process can be classified as internal and external. Internal factors relate to coal-waste composition and condition, e.g., of mineral matter (contents of quartz, feldspars, clay minerals, carbonates, and sulphides) and coal-bearing rocks (maceral composition, especially of oxidation-prone vitrinite), coal rank, moisture content, granulation, and degree of weathering. External factors include dump shape and height, convection related to atmospheric conditions, i.e., wind and rain, insolation and grain segregation (Krishnaswamy et al., 1996a, 1996b; Kaymakçi and Didari, 2002).

Self-heating and self-ignition of coal waste can be triggered spontaneously within a dump. If preventative measures are not taken, or the

* Corresponding author.
E-mail address: justyna.ciesielczuk@us.edu.pl (J. Ciesielczuk).

https://doi.org/10.1016/j.coal.2018.08.001
Received 14 April 2018; Received in revised form 31 July 2018; Accepted 3 August 2018
Available online 04 August 2018
0166-5162/

fire is not controlled at the initial stage, the fire can involve an entire dump, with serious environmental repercussions (e.g., Nadłonek and Cabała, 2016; Stracher et al., 2011, 2013, 2015). Coal is known to concentrate trace elements (e.g., Dai et al., 2003, 2004, 2005, 2012; Ward et al., 1999) which may be concentrated further by fire in coal-waste dumps (e.g., Kruszewski, 2013). Waste is not only placed in dumps, but is also used for rehabilitation or, e.g., for railway/road/river embankments where endogenic fires have been noted. Due to an increasing awareness of the dangers of self-heating, prevention- and monitoring actions have reduced the amount of burning waste. Nevertheless, cases of newly-ignited coal waste are periodically reported.

1.2. Potential of geophysical methods in research on coal fires

The electrical conductivity of loose material represented by a mixture of coal-waste rocks, mainly shales, sandstones and coal remnants, is the sum of the variety of ways in which electric charges are transported. Ionic conductivity dominates due to the presence of aqueous solutions in pore space (Kotyrba et al., 2012). During heating, the conductivity of partially saturated waste containing mixed fragments of clastic sedimentary rocks decreases due to the replacement of conductive pore water by the non-conductive fluid (air). Furthermore, at temperatures above 400 °C, clay minerals constituting the additional interface conductive component (Schön, 2015) start to release the OH group. When temperatures rise further, changes in clay minerals occur up to their disintegration or transition to other mineral phases. The importance of other conductivity types increases with increasing contents of carbon in coal, and in the waste. Laboratory experiments (Duba, 1977, 1983; Kotyrba et al., 2012) on samples of bituminous coal show the marked effect of temperature on the measured resistivity. Fresh bituminous coal is characterized by electrical resistivity of 10^3 Ωm. On heating between 20 and 60 °C, a gradual decrease in measured resistivity (down to 400 Ωm) is due to the enhanced mobility of ions in an aqueous solution. Between 60 and 100 °C, the resistivity stabilizes. Above 100 °C, a rapid increase in resistivity of several orders of magnitude occurs before a further re-stabilization level is reached. These changes are explained by the reduction of both free- and chemically-bound water contents. Above 300 °C, a further decrease in resistivity occurs, initially slow, but considerably faster above 515 °C. At a temperature of 800 °C, the resistivity of char approaches the value of 10^{-2} Ωm (Duba, 1977); these resistivity changes now relate to increasing concentrations of highly-conductive carbon.

Electromagnetic- and resistivity studies have shown a correlation of coal-seam fire zones with electrical resistivity less than several Ωm (King, 1987; Schaumann et al., 2008; Meyer et al., 2009; Revil et al., 2013; Karaoulis et al., 2014; Shao et al., 2016). Furthermore, negative self-potential anomalies are reported to exist over burning fronts (Qing and Wang, 2010; Revil et al., 2013; Karaoulis et al., 2014). Both laboratory- and field research shows these electrical parameters to be strongly dependent on the thermal processes occurring in coal-bearing rocks. In addition, during combustion, weakly-magnetic ferrous minerals such as pyrite that are common in coal seams are transformed into ferrimagnetic minerals (400-700 °C for hematite, > 500 °C for pyrrhotite, > 900 °C for magnetite), making overburned areas detectable by magnetic methods (Schaumann et al., 2008; Sant'Ovaia et al., 2010; Qing and Wang, 2010; Donelly and Bell, 2011).

Changes in resistivity comparable to those observed with fires in coal deposits can be expected in heating coal-waste dumps containing significant quantities of organic carbon. In this study, selected geoelectrical methods were tested on a thermally active dump that is not a typical coal-waste dump, but a municipal landfill where coal waste was used in its rehabilitation.

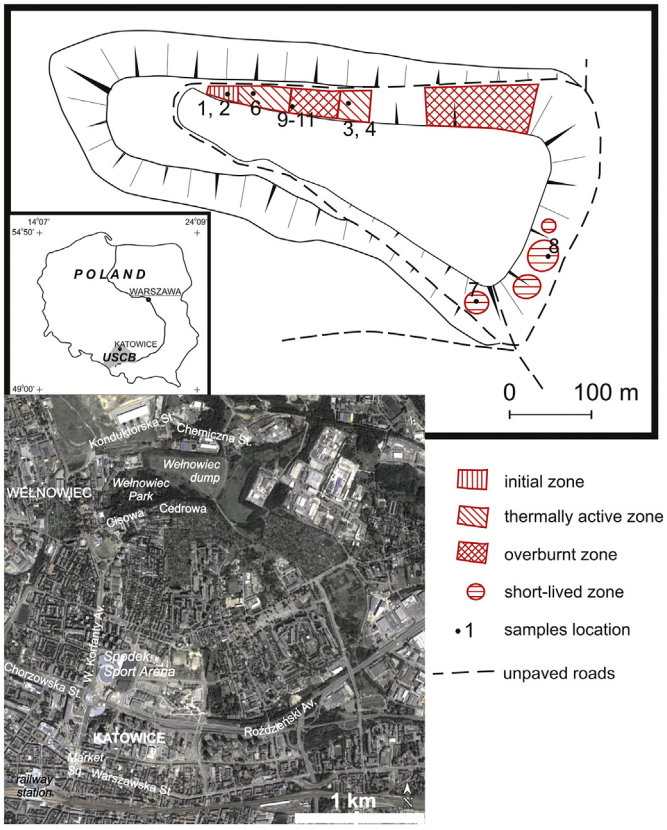

Fig. 1. The location of the Wełnowiec dump near Katowice city centre, with marked thermally-active zones and sampling sites. Numbers from 1 to 11 in figure correspond to sample codes WB1-11.

1.3. The Wełnowiec dump

The Wełnowiec dump is located ca 1 km NNE of Katowice city centre in the Upper Silesian Coal Basin. It is surrounded by housing estates and a block of flats (Fig. 1). It is a former rubbish dump for urban wastes open between 1991 and 1996. By the time of its closure, it is estimated that ca 1.6 million tons of waste had been placed in the ca 1.6 ha dump, with coal waste including sandstones, coaly shales and mudstones comprising ~22.5%, municipal waste ~21.5%, building waste ~40% and the remainder, composting plant waste. The worldwide compositions of municipal solid waste are highly variable, depending on the stage of development of the country concerned, its geographical location (climate), housing types, and methods (if any) of waste sorting (Edjabou et al., 2016). Generally, low-income countries produce higher percentages of biological waste whereas waste produced in high-income countries typically contains higher contents of paper, plastics, and metals. For example, in Scotland, a developed European country, paper and card comprise from 16 to 40%, plastics ca 4–10%, glass ca 4–5%, textiles ca 1.3–6%, metal ca 4%, and food/kitchen waste 20–30% of municipal waste (Zero Waste Scotland, Final Raport, 2010). In Ghana, the overall composition of municipal waste has been estimated to be 61% organics, 14% plastics, 5% paper, 3% metals, 3% glass, 1% leather and rubber, and 1% textiles (Miezah et al., 2015). In the Wełnowiec dump, the composition of the urban waste is as follows: paper and card ca 7%, plastics 3%, glass 3%, metal 2%, textiles 1.5%, leather and rubber 1%, and the remainder, most probably kitchen/food waste, ca 82.5%.

In 1998, after several years of usage, and complaints about odours, it was decided to rehabilitate the Wełnowiec municipal-waste landfill with coal waste from, most probably, the former “Katowice” Coal Mine nearby. A multi-barrier system was designed, a “rehabilitation layer”

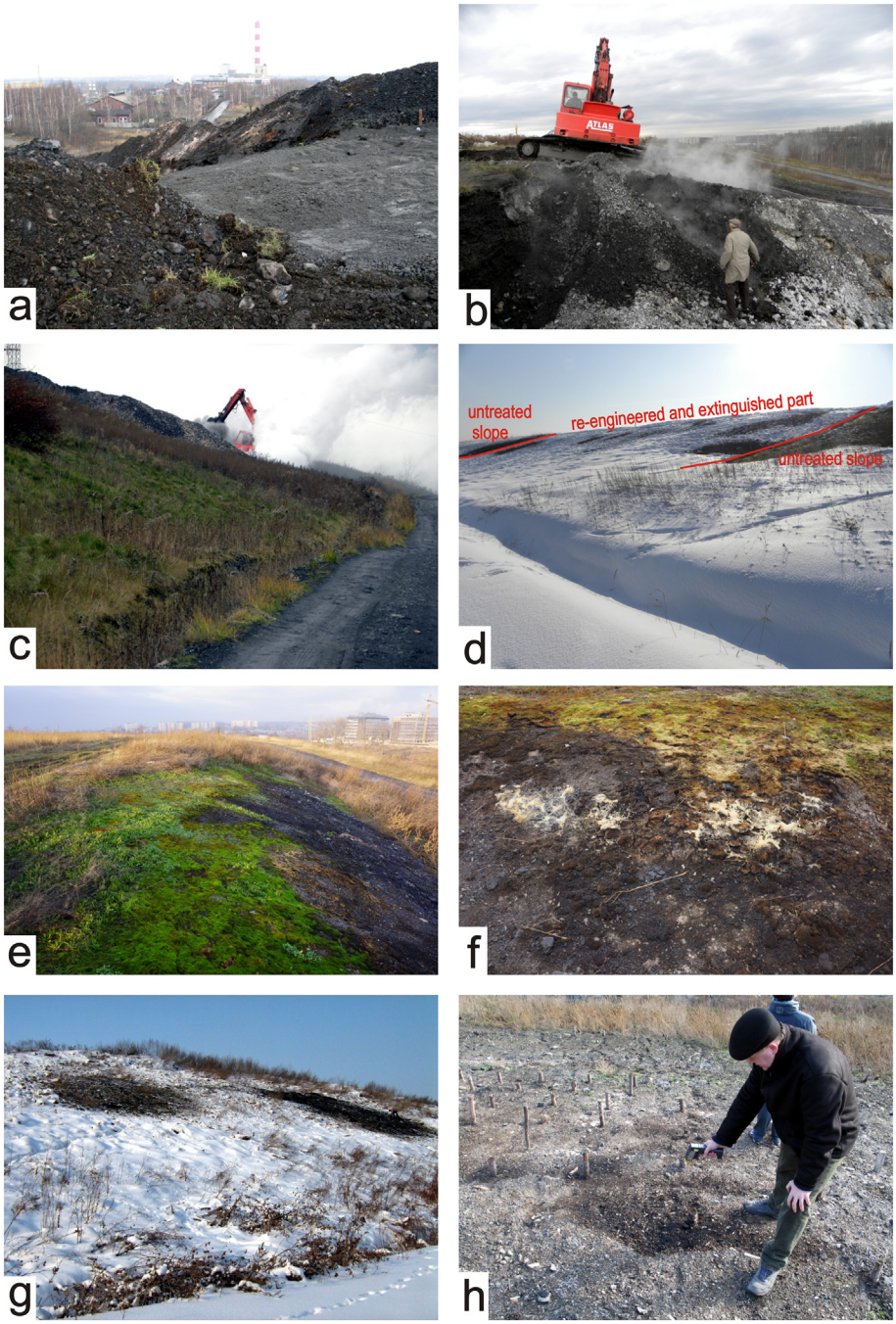

Fig. 2. The Wełnowiec municipal waste landfill rehabilitated with coal wastes which heated and ignited. A – Fire-fighting at the eastern part of the northern slope by dug 5-m deep trench filled with fly-ash slurry, December 2008. B – Coal waste of unknown excess thickness used for rehabilitation with higher than planned coal content. C – Fire-fighting in the central part of the northern slope of the dump, November 2009. D – Thermal activity within re-built and extinguished part of the northern slope, appeared on February 2010. Intensification of burning (dark spots) at the borders of extinguished area. E – Burning reaching the easternmost part of the northern slope; heated places promote vegetation growth even in winter (January 2014). F – Exhalative minerals encrusting vents on the dump surface, March 2014. G – Hot spots on the south-eastern slope of the dump: initial thermal activity ~6 m in diameter (left) and vanning activity (right), January 2010. H – Slope stabilization with wooden poles caused intensified thermal activity at the south-eastern slope of the dump. *Photos: Justyna Ciesielczuk.*

comprising, from bottom to top, 1) a 0.3 m carrier layer of compact coal-mine waste, 2) a 0.5 m sealing layer of clays, 3) a 0.1 m protective layer of sand, 4) a 0.3 m drainage layer of 16–32 mm gravel, 5) a 0.6 m layer comprising non-compacted coal-mine waste (sandstones, shales, mudstones with coal content < 5%) mixed 1:1 with soil, and 6) a 0.4 m layer of humus (Klejnowska, 1996; Ciesielczuk et al., 2013).

As the municipal waste contained 58.84 wt% of biological wastes, it was decided, in 2001, to exploit biogas (methane) from the dump (Klejnowska, 1996). A total of 39 boreholes were drilled. Though exploitation was planned for 20 years, the yield quickly became unprofitable. At that time, it was discovered that instead of the planned rehabilitation, the actual rehabilitation had used much more coal waste with much higher coal contents deposited without any packing or undertaking of fire-prevention measures (Fig. 2). The total thickness of coal waste is unknown. The rehabilitation, as might have been expected, caused self-heating and self-ignition to occur. Most likely, the dump had been self-heating for some years before the first intense fire broke out in the eastern part of the northern slope in November/December 2008 (Ciesielczuk et al., 2013). An attempt was made to extinguish the fire with fly-ash slurry. Though the fire was extinguished there (Fig. 2A), heating restarted in the central part of the same slope. Extinguishing- and re-engineering works were performed in December 2009 (Fig. 2B, C). A five-meter-deep excavation was made to isolate the burning waste zone and leave it to cool. Water and a water-lime mixture were poured over the excavation. Despite all, the action was unsuccessful, and heating was evident again in February 2010 (Fig. 2D). In fact, by admitting oxygen, the excavation works had promoted an intensification of the fire. The fire front moved slowly to reach the easternmost part of the dump in 2014 (Fabiańska et al., 2013; Ciesielczuk et al., 2013; Figs. 1 and 2E). In areas of thermal activity, vents on the

dump surface emit hot gaseous jets containing water vapour, carbon monoxide and dioxide, methane and other light hydrocarbons (Fabiańska et al., 2013Parafiniuk and Kruszewski, 2009, 2010; Kruszewski, 2013; Fig. 2F). These exhalative zones are permeated with water and bitumen formed by pyrolysis in an underlying self-heating zone. Exhalative minerals encrust many of the vents and fissures. In the vents, measured temperatures exceed 80 °C at the surface and, 0.3 m subsurface, can reach 770 °C. Heating was also observed on the eastern- and south-western slopes of the dump with hot spots reaching 500 m^2 (Figs. 1 and 2G). This activity was short-lived. Attempting of slope stabilization with wooden poles caused intensification of thermal activity (Fig. 2H).

The actual thickness of the coal waste layer, the volume of coal waste used in rehabilitation, the volume of burnt waste and the overall intensity of thermal activity at Wełnowiec are all unknown. To begin to fill this knowledge gap, geophysical-, mineralogical- and chemical investigations were carried out. Monitoring of the thermal activity of the dump by the authors since 2008 informed the choice of geophysical traverses and of representative sites for sample collection.

The main goals were to establish whether:

(a) Geophysical methods can be successfully used to detect the recent development and progression of self-heating in the coal-waste dump, and in the past.
(b) These methods could be used to distinguish municipal- and coal waste, and between burnt- and unburned coal waste.
(c) Any correlations exist between geophysical sections, chemical-, mineralogical- and petrographic coal waste characteristics and thermal activity.
(d) The planned multi-barrier system of rehabilitation was applied in any part of the Wełnowiec dump.

2. Methods

2.1. Sampling

Coal waste samples (0.5–1 kg; 10 samples in total) were collected on March 3, 2014. Samples WB3, WB4 and WB6 are from thermally-active sites on the northern slope where surface temperatures were ≤ 500 °C, vegetation was totally burnt, and the coal waste saturated with bitumen. Samples WB9-WB11 are from overburnt, porous waste of reddish-, gray- and brown colors located at the northern slope where a pit had been dug for fire-extinguishing purposes. Samples were also collected from cold sites of short-lived heating on the eastern- and south-western slope (samples WB7 and WB8) and from a site of initial burning on the western part of the northern slope (samples WB1 and WB2, Fig. 1; Table 1). Sampling focused on coal-waste material but did not include coal fragments which were dumped with the coal waste. Coal-waste samples were dried for 48–72 h at ambient temperature to an air-dry state, crushed, and homogenized for maceral analysis and XRD. Representative parts of each sample were taken for solvent extraction and leaching tests.

2.2. Organic petrography

Petrographic analyses carried out on particulate pellets included determination of maceral composition, type of maceral transformations and random reflectivity measurements. Maceral composition was determined at 500 points and reflectance measurements at 25–50 points per sample on both unaltered- and altered vitrinite particles. The number of reflectance measurements depended on the number of organic particles suitable for measurement in each sample. The maceral analyses were carried out using a Zeiss Axioplan2 reflected-light optical microscope (RLOM) with magnification 500× according to the procedure described in ISO 7404-3 (2009). For the reflectance measurements, the procedure described in ISO 7404-5 (2009) was applied.

Table 1
Representative samples from the Wełnowiec dump with locations, descriptions, extraction yields and proximate geophysical traverses.

Sample	Location	Sample description	Extraction yield [wt%]	Geophysical profile
WB1	Northern slope, dump surface, initial self-heating zone	Dark gray to gray mudstone, with weak bituminous smell and trace bitumen on the surface	1.15	EM-2
WB2	Northern slope, dump surface, initial self-heating zone	Greyish-brown mudstone, no bituminous smell	0.98	EM-2
WB3	Northern slope, dump surface, active self-heating zone	Dark to light gray with strong bituminous smell, grain size 0.2–1.5 cm	6.72	EM-2
WB4	Northern slope, dump surface, active self-heating zone	Dark gray to black with strong bituminous smell, fine grained and soft	11.69	EM-2
WB6	Northern slope, dump surface, active self-heating zone	Black, with embedded lighter particles, ~1 cm in size, with strong bituminous smell	17.22	EM-2
WB7	South-western slope, dump surface, short-lived self-heating zone	Dark gray weathered coal waste, with weak bituminous smell, grain size 0.5–2 cm	0.74	EM-1, ERT-6
WB8	South-western slope, dump surface, short-lived self-heating zone	Light gray coal waste, with visible fragments of organic matter, no bituminous smell	0.52	EM-1, ERT-5
WB9	Northern slope, in pit made during fire-extinguishing work	Dark gray and brown coal waste, with visible degassing pores, no bituminous smell	0.12	EM-2
WB10	Northern slope, in pit as for sample 7	Burnt coal waste, reddish brown in color with gray laminae, no bituminous smell	0.38	EM-2
WB11	Northern slope, in pit as for sample 7	Burnt coal waste, dark to light brown in color, no bituminous smell, grain size 0.5–2 cm	0.27	EM-2

2.3. Bitumen extraction

The samples were powdered in a rotary mortar and ca 6–12 g extracted with dichloromethane in a Thermo Scientific Dionex 350 apparatus dedicated for accelerated solvent extraction (t = 65 °C; p = 1500 psi; extraction time per sample 15 min). All solvents used were of analytical grade. Blank extractions were performed before and after the sample extractions.

2.4. Mineralogy

Mineralogical identifications were established by Powder X-ray Diffraction (PXRD) and Scanning Electron Microscopy (SEM). Phase compositions of powdered samples were determined using a fully automated X-ray Philips PW 3710 diffractometer operated at 45 kV and 30 mA, CuKα radiation, and equipped with a graphite monochromator. Mineral morphologies and spatial relationships between components were examined using a Philips XL 30 ESEM/TMP scanning electron microscope coupled with an energy-dispersive spectrometer (EDS; EDAX type Sapphire). Analytical conditions of the SEM were: accelerating voltage of 15 kV; a working distance of ca 10 mm; counting time of 40 s. All studies were carried out at the Faculty of Earth Sciences, University of Silesia, Sosnowiec, Poland.

2.5. Chemical composition of coal - waste samples and leachates

X-ray Fluorescence (XRF) was used to measure 49 element concentrations using a RIGAKU NEX DE spectrometer. Ten powdered samples were pressed and measured three times.

Atomic Absorption Spectrometry (AAS) was used to measure concentrations of selected metals in coal-waste water leachates. Powdered coal waste (15 g) in 250 cm^3 of distilled water was stirred for 2 h, left to settle for 24 h and filtered. Trace elements in the leachates were quantitatively determined using a Solaar M6 Thermo Scientific AAS spectrometer. The spectrometer working conditions were: flame type air-C_2H_2; wavelength [nm] 285.2 for Mg, 766.5 for K, 422.7 for Ca, 589.0 for Na, 324.8 for Cu, 232.0 for Ni, 213.9 for Zn, 248.3 for Fe, 240.7 for Co, 228.8 for Cd, 217.0 for Pb and 279.5 for Mn (Atomic Absorption Spectrometry. Unicam Methods Manual, 2000). Calibration curves were prepared to obtain an average absorbance for the subsequent measurements of the sample solutions.

Mobilities of the elements were calculated as the percent of the concentration of the element in the whole sample, e.g., the mobility of Mg in sample WB1 is (5.9 mg/kg *100)/3350 mg/kg = 0.18%.

2.6. Geophysics

The geophysical investigation involved 16 traverses of Electrical Resistivity Tomography (ERT); eight were sited on the flat roof of the dump, seven on slopes and one at the foot of the dump. Additionally, two traverses of shallow electromagnetic profiling (FDEM) were sited along the south-western and northern slopes (Fig. 3).

Resistivity measurements were performed with an ABEM Terrameter SAS4000 resistivity meter with 11–41 electrodes per traverse. The Wenner-Schlumberger array was applied. One of the traverses (ERT-13) with a length of 400 m and an electrode spacing of 5 m enabled the investigation to a depth of 50 m which considerably exceeded the depth of the dump. Shallow measurements with an electrode spacing of 1.5 m allowed a detailed identification of the dump structure to a depth of 4.5–10 m, depending on the length of the line. This depth was sufficient to determine the distribution of resistivity in the near-surface layer where thermal phenomena occurred, as the self-heating zones were observed at depths of 1.5–3.0 m. Each resistivity section includes at least 115 apparent resistivity measurements. Measurements were stacked 2–4 times to reach a standard deviation < 5%.

The ERT reconnaissance required the electrodes to be in direct contact with the ground, risking equipment damage in the case of extremely shallow fire-spots. Therefore, the ERT was limited to thermally inactive zones. For locations where high temperatures were expected, it was decided to make shallow electromagnetic profiling using the EM38-MK2 meter (Geonics Ltd.). This conductivity meter provides measurements of subsurface apparent conductivity at two depths simultaneously. For the applied vertical dipole configuration (VD) and 10 readings/s, the device collects information up to a depth of 1.5 m for VD = 1.0 m and to a depth of 0.75 m for VD = 0.5 m sampling the traverse at ~ 0.1 m intervals.

3. Results and discussion

Nine years of monitoring thermal activity in the Wełnowiec dump underpins the distinction of thermally-active zones that can be described as 1) initial, 2) active, 3) short-lived formerly active and 4) strongly overburnt.

The initial thermally-active zone (zone I) is where fire encroaches on new volumes of coal waste at the edges of the active zone. The thermally-active zone (zone A) encompasses areas where fire has never been extinguished and temperatures reach 400-500 °C in exhalation flues at the surface. In the short-lived formerly active areas (zone F), the fire did not last, and temperatures typically oscillated between 70 and 100 °C, with maxima of < 460 °C lasting < 1–2 months. The strongly overburnt zone (zone O) was characterized by long-lasting elevated temperatures < 800-900 °C. This zone was accessible, and sampling possible, only because burning waste had been excavated for cooling.

3.1. Maceral composition and vitrinite reflectance measurements

Organic particles are typically present in small amounts (< 5%) in the coal waste. Only in samples WB4 and WB7 the contents are higher (22.4 and 11.8%, respectively). Organic matter is absent or below the detection limit (< 0.2%) in samples WB8-WB10 (Table 2, partially published in Fabiańska et al., 2017).

Organic matter occurs as unaltered macerals of vitrinite, liptinite, and inertinite groups (Fig. 4). They are heterogeneous in terms of their origin and content. Some particles have experienced alteration due to self-heating. Low heating rates are reflected in pale-colored vitrinite also characterized by higher reflectance. Solid bitumen, a newly-formed type of organic matter, has a porous structure, dark color in reflected white light and, typically, a dark-brown fluorescence. The bitumen may occasionally host other organic particles distinguished on color, reflectance, and morphology. Chars present represent unburnt organic matter in fly ash from coal combustion in low-efficiency boilers. These forms are yellowish white in reflected white light and have high reflectance and no fluorescence. They show no signs of plasticity or are highly porous.

Samples from the initial zone (WB1 and WB2; Table 2) are strongly dominated by mineral matter (96–96.8%). Of the three maceral groups, unaltered vitrinite occurs most commonly, comprising 3% of the waste material (Fig. 4A–D). Liptinite- and inertinite macerals are rare (< 0.4%), (Fig. 4C–D). The only signs of thermal alteration are rare (< 0.4%) particles of pale-colored vitrinite. The reflectance (R_r) values are 0.81 and 0.83%, respectively.

Samples from the active thermal zone (WB3, WB4, WB6) are strongly differentiated. Two (WB3, WB6) have low organic-matter contents (< 5.6%) and WB4 is extremely rich (22.4%). Organic matter in sample WB4 is dominated by solid bitumen earlier generated from other types of organic matter. Chars are also an important component. In this case, their presence is an indication of attempts made to extinguish the fires. Inertinite and pale-colored vitrinite are much rarer (Fig. 4F). Reflectance (R_r) values are the highest of all samples (1.08%; Table 2). The organic component in samples WB3 and WB6 is dominated by unaltered macerals and chars. Solid bitumen is absent and liptinite- and inertinite macerals comprise < 0.4%. These samples are

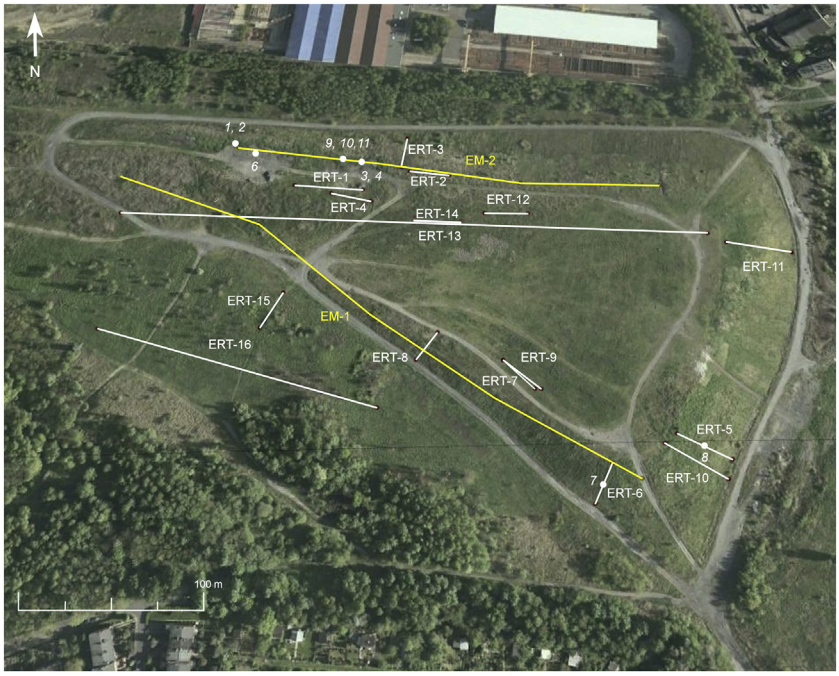

Fig. 3. Locations of geophysical traverses and sampling points.

mixed with strongly-altered (R_r = 0.92%; sample WB3) and unaltered material (R_r = 0.66%; sample WB6) occurring together. Relocation may be indicated.

Samples (WB7-WB11) from short-lived- and overburnt thermal zones represent distinct levels of waste alteration that could be related to attempts to extinguish fires and waste relocation. Both unaltered- and strongly-altered organic matter occur together. Microscopically, visible organic matter essentially absent (< 0.2%) in samples WB8-WB10 amounts to < 11.8% in samples WB7 and WB11 where it is represented by unaltered macerals (Fig. 4I–L), pale-colored vitrinite and chars (Fig. 4P). Very low R_r values (0.65 and 0.67%, respectively) possibly suggest some material relocation.

3.2. Bitumen in the Wełnowiec dump

Extraction yields are highly variable (0.12–17.22 wt%) due to a variety of processes affecting bitumen occurrence (Table 1). With both natural weathering and oxidation of coal-bearing rocks, and with leaching by meteoritic waters, bitumen content is reduced. During self-heating, the coal waste was subjected to pyrolysis increasing bitumen yield and to rapid- and severe oxygenation during firefighting activities. These processes do not equate to the natural thermal evolution within a deposit (Suggate, 1982) but rather to technological processes such as coal pyrolysis. The highest extraction yields (6.72–17.22 wt%) were found in the recent self-heating zone A, whereas the lowest (0.12–0.38 wt%) were obtained for burnt-out coal waste from the site where firefighting had taken place (zone O). Moderate values ~1 wt% typify the initial active zone I and the now inactive sites where heating had occurred in the recent past (zone F: 0.52 and 0.74 wt%). Bitumen expelled then was subjected to weathering, leaching, and evaporation; most of the pyrolysates occur at grain surfaces thus they were changed to the highest stage (Fabiańska et al., 2017).

3.3. Mineralogy

All distinguished zones touched by thermal activity result in variation in petrography and mineral composition (Table 3; Figs. 4, 5). Samples collected from a zone can differ despite their macroscopically similar appearance, as has been pointed out by coal-waste dump researchers (Ciesielczuk et al., 2014b; Ribeiro et al., 2016; Stracher et al., 2015; Sýkorová et al., 2018).

The initial thermally-active zone (zone I) is represented by greyish mudstones with a weak- or absent bituminous smell (samples WB1 and WB2). The main mineral composition, i.e., quartz, kaolinite and illite, Mg-Fe chlorites, and microcline and plagioclase, suggests that no thermal changes had taken place. Accessory monazite-(Ce) and zircon are present. Individual grains of hydroxylapatite, anatase, calcite, and spinels possibly reflect some heating (Table 3; Fig. 4A, B, C, D, 5A).

Table 2
Petrography of waste samples, Wełnowiec dump. n - number of reflectance measurements.

Sample	Thermal zone	Mineral matter [%]	Vitrinite [%]	Liptinite [%]	Inertinite [%]	Paler colored vitrinite [%]	Chars [%]	Solid bitumen [%]	R_r [%]	Standard deviation	n
WB1	Initial	96.8	3.2	0.0	0.0	0.0	0.0	0.0	0.83	0.15	50
WB2		96.0	3.0	0.2	0.4	0.4	0.0	0.0	0.83	0.29	50
WB3	Active	94.4	1.0	0.2	0.4	0.0	4.0	0.0	0.92	0.27	25
WB4		77.6	0.0	0.0	0.4	0.4	3.2	18.4	1.08	0.32	25
WB6		97.8	1.0	0.4	0.2	0.2	0.4	0.0	0.66	0.14	50
WB7	Short-lived	88.2	5.8	0.4	0.8	1.2	3.6	0.0	0.65	0.07	50
WB8		100.0	0.0	0.0	0.0	0.0	0.0	0.0	–	–	–
WB9	Over-burnt	100.0	0.0	0.0	0.0	0.0	0.0	0.0	–	–	–
WB10		100.0	0.0	0.0	0.0	0.0	0.0	0.0	–	–	–
WB11		95.0	0.8	0.0	0.0	1.6	2.6	0.0	0.67	0.09	50

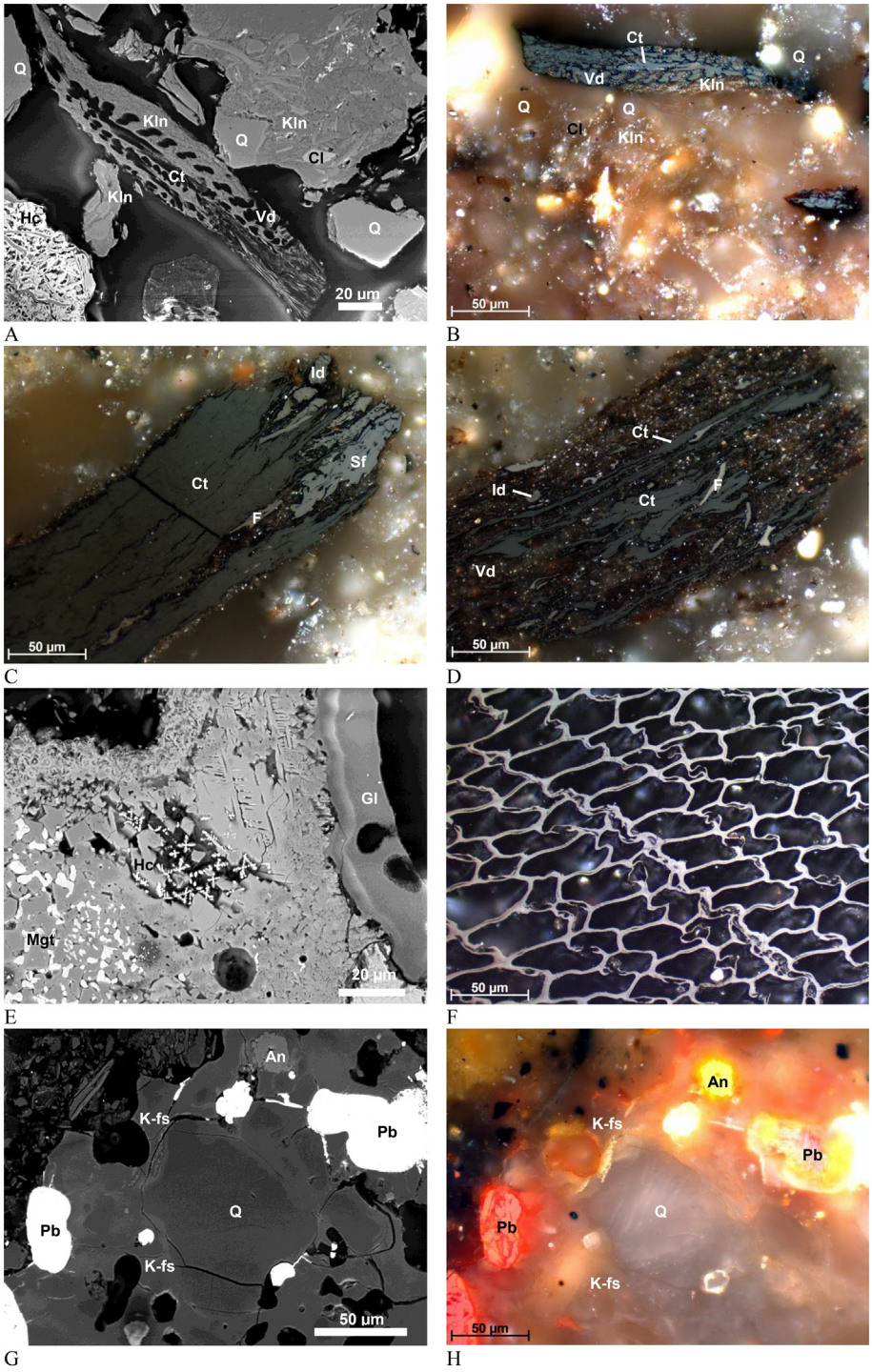

Fig. 4. Mineralogy and petrography of representative coal-waste samples. A – SEM-BSE, B – RLOM photos of sample WB1, composed of quartz (Q), kaolinite (Kln), Mg-Fe chlorite (Ch), hercynite (Hc), vitrodetrinite (Vd) and collotelinite (Ct). C – RLOM image of coal particle composed of collotelinite (Ct), semifusinite (Sf), fusinite (F), inertodetrinite (Id) in sample WB 2. D – RLOM image of particle composed of collotelinite (Ct), vitrodetrinite (Vd), fusinite (F), and inertodetrinite (Id), sample WB2. E – SEM-BSE image of sample WB3 composed of magnetite (Mgt), hercynite (Hc) and Si-Al glass (Gl). F – RLOM image of fusinite, sample WB4. G – SEM-BSE, H – RLOM images of sample WB6, composed of quartz, K-feldspar (K-fs), anatase (An) and combusted Pb. I – SEM-BSE, J – RLOM images of sample WB7, showing fusinite (F) coexisting with Fe-dolomite (Do). K – SEM-BSE, L – RLOM images of sample WB7, composed of fusinite (F), semifusinite (Sf), inertodetrinite (Id), and collotelinite (Ct) filled by kaolinite (Kln). M, N – SEM-BSE photos of sample WB9, composed of anorthite (An), spinel (Sp), hercynite, pyroxene (Px), forsterite (Fo), hydroxylapatite (Ap), celsian (Cs), and glass (Gl). O – SEM-BSE image of cordierite (Cdr) crystals grown in degassing pores, sample WB10. P – RLOM image of thermally-altered organic matter partially devolatilised (presence of large pores) and composed of semifusinite (Sf), fusinite (F) and inertodetrinite (Id), sample WB11.

A, B, C, D – zone I; E, F, G, H – zone A; I, J, K, L – zone F; M, N, O, P – zone O.

Photos: Justyna Ciesielczuk and Magdalena Misz-Kennan.

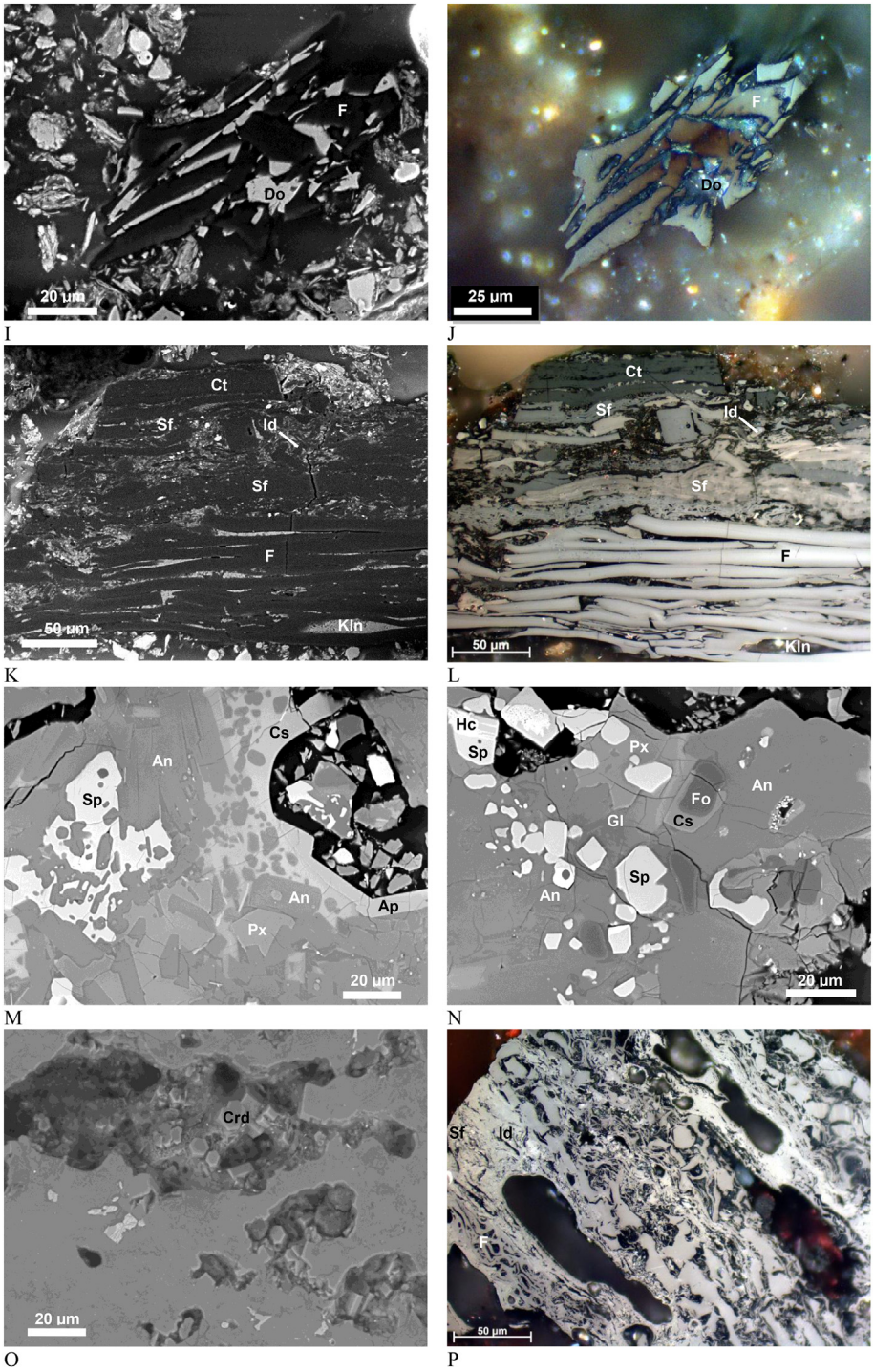

Fig. 4. (*continued*)

The thermally-active zone (zone A) is represented by waste with gray-black particles 0.2–1.5 cm in size, and with a strong bituminous smell (samples WB3, WB4, and WB6). About 90% of the waste is mineral matter. Main minerals comprise quartz, clay minerals, and feldspars. Subordinate Fe oxides, mullite, elemental lead, and a ZnS phase also occur (Table 3). However, a mixed origin is indicated by the presence of spinels (Fig. 4E); their formation requires temperatures > 800 °C which would exclude the coal present (5.6%; Fig. 4F). In fact, cenospheres from furnace combustion are ubiquitous. They were probably deposited as a rehabilitation material. Sample WB4 containing gypsum, bassanite, anhydrite and sal ammoniac was collected at an intensely-active vent. Elemental lead is a possible by-product of combustion (Fig. 4G, H, 5B). The ZnS phase (sample WB6) occurs as a coating on contemporary plants.

The short-lived thermally-active areas (zone F) are represented by gray coal waste with visible fragments of organic particles, some traces of weathering, and a weak bituminous smell (samples WB7 and WB8). The waste samples are dominated by quartz, clay minerals (illite and kaolinite), K feldspar, plagioclase, and clinochlore also present. Carbonates (calcite and dolomite) and hydroxylapatite occur as traces (Table 3; Fig. 4I, J, K, L, 5C).

The strongly-overburnt zone (zone O) is composed of reddish, gray- and brown waste (samples WB9, WB10 and WB11) with visible degassing pores and no bituminous smell. The mineralogy is very

Table 3
Mineral phase analyses (XRD and SEM-EDS) for waste samples, Wełnowiec dump.

Sample	WB1	WB2	WB3	WB4	WB6	WB7	WB8	WB9	WB10	WB11
Thermal activity zone	Initial		Active			Short-lived		Overburnt		
Quartz SiO_2	XXX	XXX	XXXX	XXXX	XXXXX	XXXXX	XXXXX		X	X
Cristobalite SiO_2									X	
Illite $(K,H_3O)(Al,Mg,Fe)_2(Si,Al)_4\ O_{10}[(OH)_2,(H_2O)]$	XXXX	XXXX	XXXX	X	XX	XX	X			
Biotite $K(Mg,Fe)_3(AlSi_3O_{10})(F,OH)_2$	EDS						EDS			
Kaolinite $Al_2Si_2O_5(OH)_4$	XX	XX	XX		XX	XX	XX			
dickite				XX						
Chlorite $(Mg,Fe)_5Al(Si_3Al)O_{10}(OH)_8$	XX	XX								
Clinochlore $Mg_5Al(Si_3Al)O_{10}(OH)_8$			X		XX	XX	X			
Microcline $KAlSi_3O_8$	XX	XX	EDS	XXX	XX		XX			
Orthoclase $KAlSi_3O_8$						XX				XX
Celsian $(K, Ba)AlSi_3O_8$								EDS		
Plagioclase $(Na, Ca)AlSi_3O_8$	X				X	EDS	XX			
Anorthite $CaAl_2Si_2O_8$								XXXX		XXXX
Cordierite $Mg_2Al_3[AlSi_5O_{18}]$									XXXXX	
Corundum Al_2O_3				EDS						
Mullite $Al_6Si_2O_{13}$			XX						XXX	
Olivine group $(Fe, Mg)_2SiO_4$								XX		
Augite								XXX		XXX
Hematite Fe_2O_3		?	EDS	EDS				X	X	X
Magnesioferrite $MgFe_2O_4$								X		
Magnetite $FeFe_2O_4$		?	EDS						X	
Hercynite $FeAl_2O_4$	EDS		EDS					EDS		
Spinel $(Mg, Fe)Al_2O_4$		EDS			?			?		X
Calcite $CaCO_3$		EDS	EDS	X	Trace	EDS				
Dolomite $CaMg(CO_3)_2$						EDS				
Gypsum $CaSO_4{\cdot}2H_2O$				XX						
Bassanite $CaSO_4{\cdot}0.5H_2O$				X						
Anhydrite $CaSO_4$				X						
Sal ammoniac NH_4Cl				X						
Hydroxylapatite $Ca_5(PO_4)_3(OH)$		EDS	EDS	EDS	Cl-EDS	EDS		X		
Zircon $ZrSiO_4$	EDS	EDS			EDS					
Monazite-(Ce) $(Ce,La)PO_4$	EDS									
Anatase TiO_2	EDS				EDS					
Lead Pb				EDS	EDS					
Iron Fe									EDS	
Chalcopyrite $CuFeS_2$									EDS	
ZnS					EDS					
Glass		?	EDS	EDS	EDS	EDS		EDS		EDS
Coal	EDS	EDS	EDS	EDS	EDS	EDS	EDS			EDS

EDS – Minerals were found by SEM-EDS but not confirmed by XRD.
XXXXX – > 50%; XXXX – 30-50%; XXX – 20-30%; XX – 7-20%; X – < 7%;? - possible.
Cl-EDS – chlorapatite according to EDS.

different; there is almost no quartz, clay minerals or K-feldspar. High-temperature minerals present include anorthite, cordierite, mullite, cristobalite, augite, olivine, Fe and Mg oxides and celsian. The last mineral is characteristic of some pyrometamorphic rocks forming in the burning coal-waste dumps, especially the so-called “black block” metapelites, i.e., fine-grained coal waste thermally transformed under low-oxygen conditions (e.g., Kruszewski et al., 2014; Ciesielczuk et al., 2015a and b; Fig. 5D). The Si and Al contents are similar (sample WB10) because of kaolinite transformation through metakaolinite and glass to mullite and cristobalite (Creelman et al., 2013). Tiny grains of metallic iron and chalcopyrite are dispersed in the matrix of sample WB10 (Table 3; Fig. 4M, N, O, P).

3.4. Chemical composition

The elements composing the collected samples occur in a wide variety of chemical forms and can vary widely. Chemical composition depends on the original composition of the coal waste, including detrital material, volcanic ash, cosmic dust, coaly material and can reflect the consequences of processes such as epigenetic mineralization, water leaching, remobilization and thermal activity. The mode of occurrence of the element dictates its behaviour and its environmental impact (Finkelman, 1993). Active fires in the coal-bearing waste can mobilize elements through direct condensation from escaping gas, interaction with coal waste, and evaporation of acidic solutions possibly enriched in metals (Křibek et al., 2017). Increasing heat first causes changes in organic matter, and then in mineral matter (Ciesielczuk et al., 2014a, 2014b and references herein). The kind and intensity of these processes are different in all of four zones and reflects the chemical and mineral composition (Tables 3 and 4). Heating or weathering has marked some changes in element contents of the raw material. Differences are evident mainly among the major elements, e.g., low Si and Al in sample WB4 reflect the high content of carbonates and sulphates in place of quartz and aluminosilicates. A single, rare mineral species in a sample can significantly increase trace-element contents, e.g., Pb (combustion-derived lead in samples WB4 and WB6), Cl (sal ammoniac in sample WB4), or ZnS in sample WB6.

Increased- or decreased amounts of elements (in bold or underlined, respectively, in Table 4), e.g., Mg, P, Ca, Mn, Fe, Zn, Ag, Sn, Sb, Co, Pb, Se, REE, Te, I and Ta relate mainly to active- and overburnt sites. Heating triggers element mobility mainly by changes of mineral phases, as the amount of coal in the waste is small. The unusually high amount of Mg in overburnt samples is due to pyroxene. Heating causes hematite, magnetite, and magnesioferrite to form, leading to increased Fe and Mg, and increases in trace elements showing affinity to them, e.g., Co, As, Sn and Ge. Extremely high Ca in burnt waste is due to anorthite.

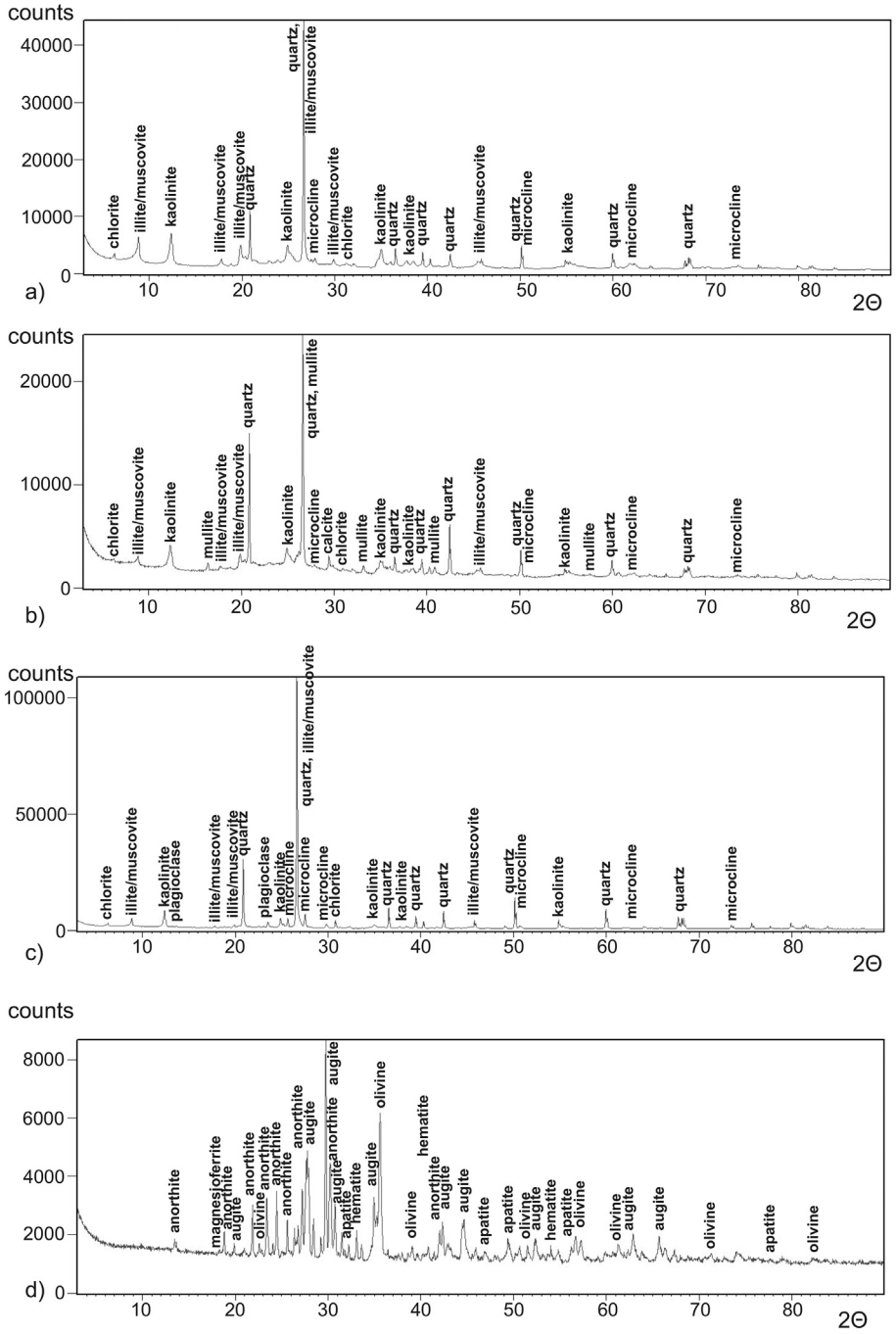

Fig. 5. PXRD patterns of representative samples. A – Initial thermal zone (sample WB2). B – Active zone (sample WB3). C – Short-lived active zone (sample WB8). D – Overburnt zone (sample WB9).

As K-feldspar in zone O contains celsian, so Ba and associated Sr increase. Interestingly, in samples showing REE enrichment, La is clearly elevated only in samples WB9 and WB11, whereas Nd is dominant in samples WB6, WB8, WB9, and WB11.

The Si, Al, K, Ca, P, S, Cl, Mn, V, Tl, Sn, Co, Fe and Rb contents in the samples (Table 4) closely reflect their different mineralogies (Table 3). The presence of carbonates and lower contents of quartz, aluminosilicates, and glass is reflected in an increase of Ca and decreases in Si and Al. Higher P is linked to the presence of an apatite group species. High Ca and S in sample WB4 is due to the presence of weathering minerals, namely gypsum, bassanite and anhydrite and high Cl to the occurrence of sal ammoniac in thermally active areas. Mn, Ag, Sn, and Co, with their affinity to Fe, reflect the presence of Fe oxides, and vanadium and thallium the presence of clay minerals. There is no correlation of Rb with the presence of K-feldspar in the dump although some affinity to illite is noted, as in the Starzykowiec coal-waste dump (Ward, 2002, 2016; Ribeiro et al., 2010; Ciesielczuk et al., 2014a; Křibek et al., 2017). Invariable amounts of other elements reveal nothing of the thermal activity.

In general, the chemistries of the initial I and short-lived F zones are similar and differ from those of the thermally active A and overburnt O zones (Table 4, in bold, last four columns). The contents of Si, Ti, Al, K, Sb, In, and Sc are significantly higher whereas those of Fe, Mn, Mg, Ca, P, Sr, Ba, Se, Ce, Pr, Nd, Sn, Te, and I are lower. The effects of long-lasting thermal activity are obvious.

Table 4
Chemical composition [mass %; XRF] of waste samples, Wełnowiec dump. Increased values are in bold and decreased values are underlined.

Thermal zone	WB1	WB2	WB3	WB4	WB6	WB7	WB8	WB9	WB10	WB11	Possible cause or mode of occurrence	Averages			
	Initial zone		Active zone			Short-lived zone		Overburnt zone				Initial	Active	Short-lived	Over-burnt
Si	25.1	24.5	21	13.9	23.4	23.6	29	19.7	27.3	19.6	Carbonates, sulphates, depletion in quartz	**24.80**	19.43	**26.30**	22.20
Ti	0.54	0.58	0.539	0.386	0.351	0.546	0.291	0.307	0.516	0.277	Affinity to anatase and zircon	**0.56**	0.43	**0.42**	0.37
Al	5.66	6.03	5.61	2.52	4.02	5.36	4.05	5.2	5.14	4.74	Carbonates	**5.85**	4.05	**4.71**	5.03
Fe	1.68	1.6	2.8	1.64	**3.78**	1.63	1.34	**9.86**	**6.01**	**5.86**	Fe oxides	1.64	**2.74**	1.49	**7.24**
Mn	0.0288	0.023	0.0503	0.0542	0.0585	0.029	0.0316	**0.222**	**0.143**	**0.132**	Fe oxides	0.03	**0.05**	0.03	**0.17**
Mg	0.335	0.327	0.911	0.265	0.245	0.25	0.225	**2.14**	0.549	**1.559**	Augite	0.33	**0.47**	0.24	**1.42**
Ca	0.211	0.321	**1.63**	**5.68**	**0.737**	0.353	0.217	**8.63**	0.205	**5.2**	Calcite, augite, anorthite	0.27	**2.68**	0.29	**4.68**
K	2.59	3.02	2.02	1.26	1.72	2.5	3.31	0.957	2.94	1.33	Depletion in illite and K feldspar	**2.81**	1.67	**2.91**	1.74
P	0.143	0.148	**0.308**	**0.459**	0.133	0.14	0.134	**0.317**	0.155	0.281	Apatite	0.15	**0.30**	0.14	**0.25**
S	0.214	0.167	0.142	**4.01**	0.253	0.174	0.1042	0.113	0.104	0.192	Gypsum, ZnS	0.19	**1.47**	0.14	0.14
Cl	0.0541	0.0432	0.0515	**1.67**	0.0574	0.0475	0.0427	0.0605	0.0486	0.0594	Salammoniac, chlorapatite	0.05	**0.59**	0.05	0.06
V	0.0297	0.0334	0.041	< 0.0001	0.0058	0.03	0.0128	0.008	0.035	0	Affinity to illite	0.03	0.02	0.02	0.01
Cr	0.0244	0.0273	0.0295	0.0175	**0.133**	0.0303	0.0198	0.0195	0.0352	0.001	Affinity to chlorite and spinel	0.03	0.06	0.03	0.02
Co	0.0122	0.0114	0.0176	0.0122	**0.0241**	0.0127	0.0103	**0.0487**	**0.0318**	**0.0304**	Affinity to Fe oxides	0.01	0.02	0.01	0.04
Ni	0.0195	0.0208	0.0222	0.021	0.0398	0.0202	0.0201	0.0282	0.0223	0.0193		0.02	0.03	0.02	0.02
Cu	0.0085	0.0089	0.0108	0.0263	0.0132	0.0091	0.0065	0.0178	0.0112	0.0114		0.01	0.02	0.01	0.01
Zn	0.0085	0.0079	0.023	**0.0916**	**0.181**	0.0225	0.0084	0.005	0.0132	0.0061	ZnS	0.01	**0.10**	0.02	0.01
As	0.0011	0.001	0.0016	0.0015	0	0.0012	0.0008	0.0008	0.0009	0.0003	Affinity to hematite	0	0	0	0
Rb	0.0127	0.0161	0.0121	0.0061	0.008	0.0117	0.0107	0.0052	0.0153	0.007	Affinity to illite	0.01	0.01	0.01	0.01
Sr	0.0098	0.0136	0.0472	0.0217	0.0082	0.011	0.0078	**0.095**	0.0105	0.0539	Celsian	0.01	**0.03**	0.01	**0.05**
Mo	0	0	0	0.0027	0.0158	0	0	0	0	0.0014	ZnS	0	0.01	0	0
Cd	0.0016	0.0013	0.0014	0.0017	0.0043	0.0018	0	0	0.0013	0.005	ZnS	0	0	0	0
Sb	**0.202**	< 0.0001	0.0405	0.0009	**0.1138**	**0.194**	**0.263**	0.0475	**0.163**	0.0069	Hercynite, coal, plagioclase, ZnS, chalcopyrite, iron	**0.10**	0.05	**0.23**	0.07
Ba	0.0506	0.065	0.0752	0.0651	0.1504	0.0593	0.1186	**1.023**	0.0622	0.503	Celsian	0.06	**0.10**	0.09	**0.53**
Pb	0.0028	0.0034	0.0071	**0.0253**	**0.163**	0.0075	0.0024	0.0012	0.002	0.005	Combusted Pb	0	**0.07**	0	0
Se	< 0.0001	< 0.0001	0.0005	**0.0338**	0.0002	0	0	**0.0281**	0	0	ZnS, lead, gypsum, coal	0	**0.01**	0	**0.01**
Hg	0	0	0	0	0.0036	0	0	0	0	0.0019	ZnS, coal	0	0	0	0
Y	0.0055	0.0056	0.0056	0.0007	0.0066	0.0046	0.0039	0.0071	0.0065	0.0064	Carbonates, apatite	0.01	0	0	0.01
Hf	0.0008	0.0031	0.0038	0.0039	0.0036	0.004	0.0038	0.004	0.0038	0.003		0	0	0	0
Nb	0.0033	0.0032	0.0031	0.0017	0.0016	0.0024	0.0015	0.003	0.0031	0.0023	TiO_2, zircon	0	0	0	0
Ta	0	0.0008	0.0024	0.0014	0.0026	0.0017	0.0032	**0.0056**	0.001	**0.0044**	Augite, plagioclase	0	0	0	0
Th	0.0017	0.0019	0.0019	0.001	0.0019	0.002	0.001	0.0019	0.0018	0.0017		0	0	0	0
U	0.0004	0.0004	0.0004	0.0001	0	0.0003	0.0001	0.0007	0.0003	0.0004		0	0	0	0
La	0.0002	0.0002	< 0.0001	0	0	0.0263	0.0203	**0.113**	0	**0.1012**		0	0	0.02	0.07
Ce	0.0058	0.0057	0.0034	**0.0574**	**0.078**	0.0031	**0.0493**	**0.142**	0.0041	**0.129**		0.01	**0.05**	0.03	**0.09**
Pr	< 0.0001	< 0.0001	< 0.0001	**0.0517**	**0.0784**	0.0001	**0.0693**	**0.0595**	0	**0.1018**		0	**0.04**	0.03	**0.05**
Nd	0.0036	0.0065	0.0043	0.0043	**0.1232**	0.0037	**0.0854**	**0.232**	0.0044	**0.197**		0.01	**0.04**	0.04	**0.14**
Dy	0.0132	0.0151	0.0222	0.0152	0.0205	0.0148	0.0162	0.0269	0.0228	0.0187		0.01	0.02	0.02	0.02
Br	0	0	0.0007	0.0098	0	0.0006	0	0	0	0	Sal ammoniac	0	0	0	0
Rh	0.0005	0	0	0	0	0	0	0	0	0		0	0	0	0
Ag	0.0003	0.0002	0.0002	0.0008	0.0021	0.0003	0.0012	**0.0035**	0.0003	**0.0029**	Magnesioferrite, spinel	0	0	0	0
Sn	0.0013	0.0011	0.0049	0.0051	0.0069	0.0016	0.0044	**0.0106**	**0.0796**	**0.0108**	Affinity to Fe oxides	0	**0.01**	0	**0.03**
W	0.0034	0.003	0.0012	0	0.0191	0	0	0	0.0039	0.004		0	0.01	0	0
Ir	0.0024	0.0021	0.0024	0.0024	0.0035	0.002	0.0022	0.0024	0.0024	0.0018		0	0	0	0
Pt	0.0017	0.0018	0.0015	0.0025	0.003	0.0022	0.0016	0	0.0024	0		0	0	0	0
Au	0	0.0004	0.0014	0.0023	0.0035	0	0.0018	0.0014	0.0005	0		0	0	0	0
Ga	0.0027	0.0032	0.0028	0.0016	0.0013	0.0028	0.0013	0.0019	0.0032	0.0012	Spinel, plagioclase, coal	0	0	0	0
Ge	0.0926	0.119	0.0011	**0.181**	0.001	0.118	0.0941	**0.1677**	0.12	**0.214**	Affinity to Fe oxides	0.11	0.06	0.11	0.17
In	0.561	0.73	0.545	0.465	0.463	0.568	0.691	0.398	0.455	0.308		**0.65**	0.49	**0.63**	0.39
Te	0.149	0.27	0.314	**0.658**	0.1569	0.219	0.221	**0.894**	0.145	**0.76**		0.21	**0.38**	0.22	**0.60**
I	0.0008	0	0.0005	**0.0112**	0.037	0.0007	0	**0.0097**	0	**0.0187**	Sal ammoniac	0	**0.02**	0	**0.01**
Cs	< 0.0001	0	0	0	0	0	0	0	0	0		0	0	0	0
Tl	0.0012	0.0011	0.0013	0	0	0	0.0016	0	0.0015	0	Clay minerals	0	0	0	0
Sc	0.0103	0	< 0.0001	< 0.0001	0.0036	0.0216	0	0	0.0069	0		**0.01**	0	**0.01**	0

Table 5
Comparison of rock sample and leachate [mg/kg] compositions and mobility of selected elements [%] with outstanding values in bold.

	Thermal zone	Mg			K			Ca			Na	Mn			Fe			Mg + K + Ca + Mn + Fe		
		Rock mg/kg	Leachate mg/kg	%	Rock mg/kg	Leachate mg/kg	%	Rock mg/kg	Leachate mg/kg	%	Leachate mg/kg	Rock mg/kg	leachate mg/kg	%	Rock mg/kg	Leachate mg/kg	%	Rock mg/kg	Leachate mg/kg	%
WB1	Initial	3350	5.9	0.18	25900	70	0.27	2110	24	1.13	104.02	288	b.l.	0.00	16800	0.14	0.00	48450	99.44	0.21
WB2		3270	53	1.62	30200	317	1.05	3210	305	9.51	84.17	230	b.l.	0.00	16000	0.38	0.00	52900	675.51	1.28
WB3	Active	9110	61	0.67	20200	139	0.69	16300	276	1.69	60.96	503	0.24	0.05	28000	0.22	0.00	74100	476.76	0.64
WB4		2650	**1090**	**41.26**	12600	**1060**	**8.43**	**56800**	**20700**	**36.47**	**795.06**	542	25	**4.55**	16400	0.25	0.00	88100	22893.97	**25.73**
WB6		2450	77	3.14	17200	196	1.14	7370	478	6.49	142.50	585	0.01	0.00	37800	0.10	0.00	65400	10562.51	1.15
WB7	Short-lived	2500	32	1.28	25000	221	0.89	3530	242	6.87	63.68	290	b.l.	0.00	16300	0.10	0.00	47600	750.86	1.04
WB8		2250	58	2.58	33100	203	0.61	2170	611	**28.16**	79.98	316	b.l.	0.00	13400	1.9	0.01	51200	496.04	1.71
WB9	Over burnt	**21400**	49	0.23	9570	45	0.47	**86300**	565	0.65	26.84	**2220**	b.l.	0.00	**98600**	0.41	0.00	218100	874.53	0.30
WB10		5490	25	0.46	29400	109	0.37	2050	95	4.61	54.22	**1430**	0.87	0.06	**60100**	2.0	0.00	98500	658.80	0.24
WB11		**15590**	452	2.90	13300	451	3.39	**52000**	**13300**	**25.62**	133.79	**1320**	0.53	0.04	**58600**	b.l.	0.00	140800	232.00	**10.10**
Averages																				
Initial		3310	30	0.90	28,050	193	0.66	2660	165	5.32	94.09	259	0.00	0.00	16,400	0.26	0.00	50,680	387.48	0.76
Active		4737	411	15.03	16,667	466	3.42	26,823	7160	14.88	332.84	543	8.3	1.53	27,400	0.19	0.00	76,170	8040.53	10.56
Short-lived		2375	45	1.93	29,050	212	0.75	2850	427	17.52	71.83	303	0.00	0.00	14,850	1.0	0.01	49,430	685.28	1.39
Overburnt		14,160	175	1.19	17,423	202	1.41	46,783	4660	10.30	71.62	1657	0.47	0.03	72,433	0.79	0.00	152,500	5039.00	3.31

	Thermal zone	Ni			Cu			Zn			Cd		Pb		Co			Ni + Cu + Zn + Cd + Pb + Co		
		Rock mg/kg	Leachate mg/kg	%	Rock mg/kg	Leachate mg/kg	%	Rock mg/kg	Leachate mg/kg	%	Rock mg/kg	Leachate mg/kg	Rock mg/kg	Leachate mg/kg	Rock mg/kg	Leachate mg/kg	%	Rock mg/kg	Leachate mg/kg	%
WB1	Initial	195	b.l.	0.00	85	0.31	0.36	85	0.07	0.08	16	b.l.	28	b.l.	122	0.10	0.08	531	0.48	0.09
WB2		208	b.l.	0.00	89	0.40	0.44	79	0.06	0.08	13	b.l.	34	b.l.	114	0.02	0.02	537	0.47	0.09
WB3	Active	222	b.l.	0.00	108	0.86	0.80	230	0.54	0.24	14	b.l.	71	b.l.	176	b.l.	0.00	821	1.41	0.17
WB4		210	0.66	0.32	263	0.36	0.14	**916**	**3.72**	0.41	17	b.l.	**253**	b.l.	122	0.03	0.03	1781	4.77	0.27
WB6		398	b.l.	0.00	132	0.34	0.26	**1810**	0.20	0.01	43	b.l.	**1630**	b.l.	241	0.21	0.09	4254	0.76	0.02
WB7	Short-lived	202	b.l.	0.00	91	0.35	0.39	225	0.11	0.05	18	b.l.	75	b.l.	127	0.28	0.22	738	0.75	0.10
WB8		201	b.l.	0.00	65	0.92	1.41	84	0.38	0.46	-	b.l.	24	b.l.	103	0.01	0.01	477	1.31	0.27
WB9	Over burnt	282	b.l.	0.00	178	0.21	0.12	50	0.22	0.45	-	b.l.	12	b.l.	487	b.l.	0.00	1009	0.44	0.04
WB10		223	b.l.	0.00	112	**4.22**	**3.77**	132	0.29	0.22	13	b.l.	20	b.l.	318	0.17	0.05	818	4.68	0.57
WB11		193	b.l.	0.00	114	0.56	0.49	61	0.47	0.77	50	b.l.	50	b.l.	304	0.22	0.07	772	1.26	0.16
Averages																				
Initial		202	–	–	87	0.35	0.40	82	0.06	0.08	15	–	31	–	118	0.06	0.05	534.00	0.48	0.09
Active		277	0.22	0.11	168	0.52	0.40	985	1.49	0.22	25	–	651	–	209	0.11	0.04	2285.33	2.31	0.10
Short-lived		202	–	–	78	0.63	0.90	155	0.25	0.25	9	–	50	–	115	0.15	0.12	607.50	1.03	0.17
Overburnt		233	–	–	135	1.67	1.46	81	0.33	0.48	21	–	27	–	370	0.13	0.04	866.33	2.12	0.25

b.l. – below detection limit.

3.5. Metal concentrations in coal-waste leachates

Concentrations of major (Mg, K, Ca, Na, Mn, Fe) and minor (Ni, Cu, Zn, Cd, Pb, Co) elements were measured in leachates from samples from the four zones of thermal activity in the dump (Table 5). Selected elemental compositions and percentages of elements in leachates compared to those in corresponding whole samples are shown in Table 5. Some, such as Ni, Cd, and Pb, are below the detection limit, while Fe, Zn and Co are < 1% of their sample contents. Clearly, they were not activated by water at any thermally-active site, and their mobility from coal waste was not affected by fire (Ribeiro et al., 2010). This supports the contention that their mobility depends on the chemical- and physical properties of the mineral phase with which it is associated. Furthermore, the overburnt coal-waste material is much more inert than "fresh" waste. Coal waste at the burning stage is the most environmentally aggressive (Křibek et al., 2017; Sýkorová et al., 2018). The most important metals appearing in high concentrations in the leachates are K, Ca and Na. Magnesium appears in lower amounts. The highest concentrations of Mg, K, Ca Na, Mn, and Zn in the leachate of sample WB4, and the abundant Cu and Fe in that of sample WB10 (Table 5, in bold) imply that the leachates collected only metals forming water-soluble mineral phases such as sulphates (gypsum, bassanite, anhydrite) and sulphides ($CuFeS_2$) that crystallized during fire or weathering. High concentrations of Pb in samples WB4 and WB6, and its absence in leachates, reflect the presence of insoluble combusted lead.

The highest water-leachable concentrations of elements occur in the active A and overburnt O zones. In the short-lived thermally-active sites, concentrations are also relatively high. Low concentrations are likely due to scarcity/lack of an element in the waste or occurrence only as an insoluble mineral, e.g., native lead (sample WB6) and Fe oxides in all. However, concentrations are highly variable and any correlations with thermal activity unsure.

3.6. The structure of the dump established by the geoelectrical field measurements

Resistivity imaging was carried out through all thermal zones and areas not affected by thermal phenomena on the dump surface (ERT-1, 2, 4, 7, 9, 12, 13, and 14), slopes (ERT-3, 5, 6, 8, 10, and 11) and surroundings (ERT-15 and 16).

The imaging for the longest W-E traverse (ERT - 13), extending to a depth of 50 m and considerably exceeding the thickness of the dump, establishes the actual thicknesses of the urban waste and of the rehabilitation layer. The waste was deposited on Lower Pennsylvanian (Namurian B) sandstones and mudstones (Flötzkarte des Oberschlesischen Steinkohlenbeckens, 1903). Bore-hole logs show that the roof of the bedrock (Kinderscoutian-Marsdenian) is at 278–283 m a.s.l. Atlas Geologiczno-Inżynierski Aglomeracji Katowickiej (http://bazadata.pgi.gov.pl/data/atlasy_gi_otwory). It correlates with the shape of 50 Ωm isoohm in the ERT-13 resistivity section (Fig. 6). Logs indicate that the roof of the bedrock is composed of strongly-weathered rocks, which explains its relatively low resistivity.

The urban waste consists of mixed municipal refuse (~30%), rubble and soil (~40%) and coal waste (~22.5%) lying on a layer of slag, ash and bricks (Klejnowska, 1996; Atlas Geologiczno-Inżynierski Aglomeracji Katowickiej http://bazadata.pgi.gov.pl/data/atlasy_gi_otwory). The ERT-13 section shows its thickness to be ~20 m. The resistivity of the waste is below 30 Ωm.

According to the plan proposed for the dump rehabilitation, a 2.2 m rehabilitation layer was to be composed mainly of coarse-grained material including coal waste. The coal-bearing rocks were to be < 5% (Ciesielczuk et al., 2013). The ERT-13 section shows that the rehabilitation layer varies in thickness from 2 to 8 m. Its resistivity typically ranges from 50 to 80 Ωm but, to the east of the dump, locally exceeds 200 Ωm, probably related to the raised content of coal waste used. In the eastern half of the section, the resistivity of the rehabilitation layer is like that of the Lower Pennsylvanian bedrock. Considerably lower resistivity (≤ 20 Ωm) noted near the surface in the western- and central parts (intervals: 105–165 m and 182–192 m) of ERT-13 (Fig. 6) reflects the presence of sewage sludge used for firefighting on the northern slope.

The rehabilitation project for the cover envisaged a multi-barrier system composed of carrier-, sealing-, protective-, drainage-, coal waste- and humus layers. A correctly-made multilayer system should be detectable especially on the flat plateau on the dump top. Detailed measurements (ERT-9, ERT-12, ERT-14) with electrodes separation of 0.75 m and a multiple-gradient array performed on the dump roof reveal (Fig. 7) reveals no layered structure. There are no regular vertical changes in resistivity; the most obvious variability is horizontal and related to the lateral distribution of material.

To check the thickness of the rehabilitation layer, short ERT lines with an electrode spacing of 1.5 m were set out on the roof and on the slopes of the dump (Fig. 3). For most of the ERT sections for the northern part of the roof (ERT-1, ERT-4, ERT-12), the rehabilitation layer is ~2–3 m thick (Fig. 8A), and even thinner for ERT-14 (Fig. 7) and ERT-7 (Fig. 8B) on the southern part of the roof. Urban waste appears in the bottom part of both sections a and b in Fig. 8. The coal waste on the roof never self-ignited; possibly the thin layer allowed more rapid heat dispersion. Locally, on the roof of the dump, the thickness of the rehabilitation layer increases considerably, e.g., in the eastern part of the ERT-13 section (Fig. 6) and the entire ERT-2 section (Fig. 8C). The section shown in Fig. 8C pertains to the northern edge of the roof in the area adjoining the thermally-active zone A. This section does not reach the roof of the low-resistivity municipal waste at a depth of 4 m; the thickness of the rehabilitation layer much exceeds the thickness planned.

As the thermal phenomena developed only on the dump slopes, the remaining traverses were located there, mostly in areas of extinguished- and current thermal activity. ERT-3 is in the inactive area in the immediate vicinity of the active zone. ERT-5, ERT-6, and ERT-10 cross the old fire areas (zone F) on the eastern- and south-western slopes (Ciesielczuk et al., 2013). ERT-8, ERT-11 and ERT-15 cross slopes that have never been thermally active.

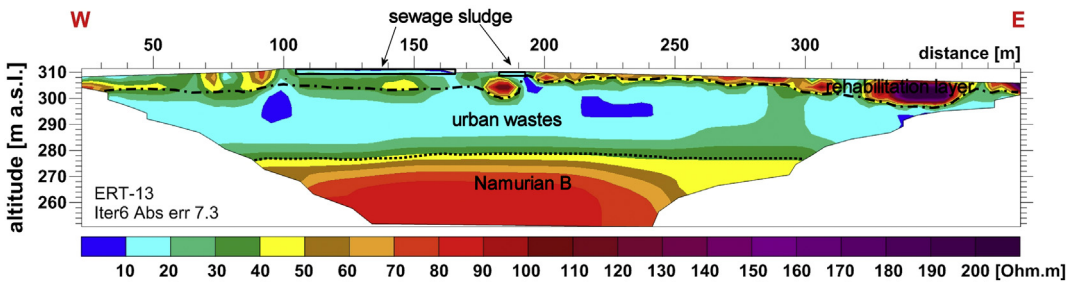

Fig. 6. Deep geoelectrical section obtained for ERT-13 traverse. Dashed line is the interpreted roof, and the dotted line the interpreted floor, of the urban waste. Rectangles are the sewage sludge used in the last stages of firefighting.

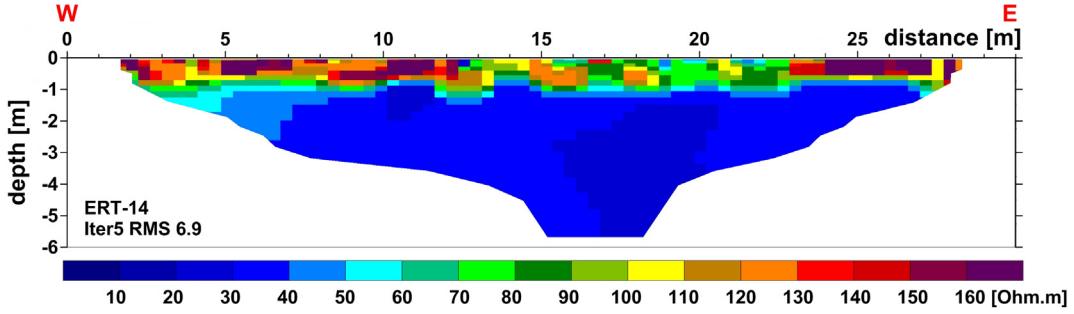

Fig. 7. Geoelectrical section (model blocks) for ERT-14 traverse.

In places, the rehabilitation layer is thicker on the slopes than on the dump roof. Resistivity values characteristic of rehabilitation layer extend locally to a depth of 4.5 m at least, twice exceeding the planned thickness of the rehabilitation layer. Contents of material with high resistivity are also greater in the slope rehabilitation layer compared to the roof. According to our observations during firefighting activities on the northern slope, the entire rehabilitation layer consists of coal waste with no sign of a multi-layer barrier system.

For the ERT-8 section on the south-western slope within the area which was never affected by heating (Fig. 9A), the resistivity of the rehabilitation layer ranges from 50 to 200 Ωm and the maximum thickness of the rehabilitation layer, i.e., 2.5 m, is seen at the base of the slope. In the upper part of the slope, only the urban waste is evident. This could be the result of gravitational separation of newly-deposited material during the rehabilitation or later down-slope creep.

For the ERT-3 (Fig. 9B) traverse over the inactive part of the northern slope, the rehabilitation layer is continuous and no thicker than 2 m. The high-resistivity part of the rehabilitation layer with a thickness < 1 m is distributed evenly along the slope. ERT-15 reveals a similar pattern.

For traverses ERT-6 (Fig. 9C) on the south-western slope, and ERT-5 (Fig. 9D) and ERT-11 (section not figured) on the eastern slope, the thickness of the rehabilitation layer exceeds 4–4.5 m. It was shown by Dulewski et al. (2010) that fire risk increases for coal waste thicker than 4 m. Despite the thickness of the rehabilitation layer along ERT-11, the authors have not seen any thermal activity since the autumn of 2008. The ERT-6 section reaching a depth of 5 m does not reach the roof of municipal waste. In the central part (10–18 m) of the rehabilitation layer, the area of the highest resistivity is absent on this south-western slope. There, a fire spot (zone F) was observed in January 2010 and a temperature of 320 °C measured at a depth of 0.3 m (Ciesielczuk et al., 2013).

In the formerly active ERT-5 section, the thickness of the rehabilitation layer varies and areas of resistivity > 100 Ωm appear only locally (Fig. 9D). In the nearby ERT-10 section, where some heating was noted in 2009, the structure of the shallow layer of high resistivity is as in ERT-6, despite the small thickness of the rehabilitation layer.

Breaks of the rehabilitation layer in the upper parts of un-reconstructed slopes (ERT-8, ERT-5, and ERT-10) may be an indicator of mass movement. After rehabilitation, the designed slope of the dump was 14° to the N, 18° to the S and 20° to the E. For coal waste with 5–30% of dust- and clay fractions, the internal friction angle ranges from 38.97–35.34° (Zapał and Ratomski, 2007). Slopes made of such coal waste should be stable up to 28.6°. Today, average measured slopes are 18° to the north (ERT-3; covered by sewage sludge), 22-23° to the east (ERT-5 and ERT-10) and range from 10° (ERT-15) to 20° (ERT-8, ERT-6) to the south. Inclinations are not constant along slopes. The greatest inclination approaching 24.5°, is observed in the central parts of slopes (ERT-3, ERT-5, ERT-6, and ERT-10). It appears from the measurements that the slopes, though slightly steeper than designed, do not exceed the critical value. Despite this, slope instability may still occur. A few years exposure, especially to rain, increases coal-waste porosity and result in a reduction of the internal friction angle to 20°, likely triggering slope instability. Speculations about mass movement along the slopes are supported by observations made by the authors; before thermal activity became apparent, some evidence of slope-stabilization work was noted in 2006–7 near the SE corner of the dump.

Combustion in coal beds and coal waste exposed to air and water due to rock-mass wasting or rapid erosion has been reported from the USA (Heffern and Coates, 2004, Martínez et al., 2009 after Lyman and Volkmer, 2001), Canada (Sanei et al., 2013), India (Prakash et al., 2013), Portugal (Ribeiro et al., 2013) and Venezuela (Soto and Urbani, 2015). In the Wełnowiec dump, breaks in the rehabilitation layer may indicate slope failure with the slip plane potentially coinciding with the border between mining waste and urban waste. Any resulting access of water and air might well aid initiation of heating. A spatial correlation seems to link landslides and cracks in the upper parts of the slopes with heating; it is there that fire-related exhalations are prone to be emitted (Ciesielczuk et al., 2013).

The ERT measurements are supplemented by two electromagnetic traverses EM-1 and EM-2, 400 and 300 m long respectively, on the upper parts of the south-western and northern slopes of the dump

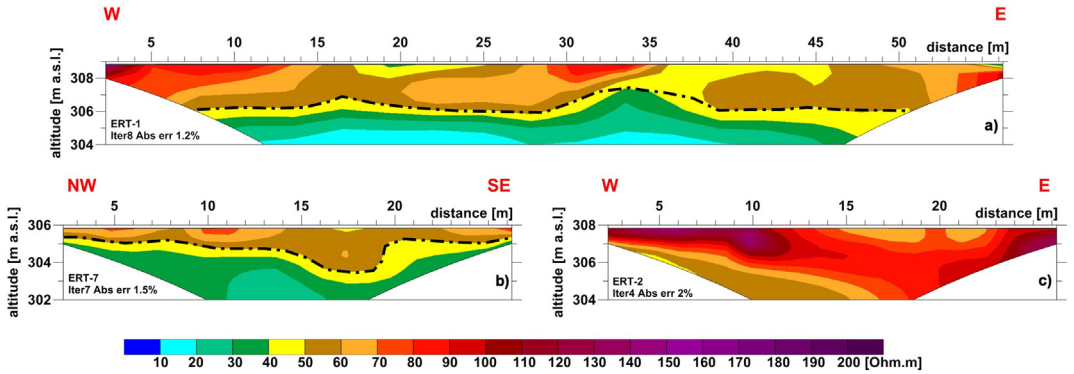

Fig. 8. ERT sections for selected traverses on the top of the dump. Dashed line is the interpreted roof of the urban waste. A – ERT-1. B – ERT-7. C – ERT-2.

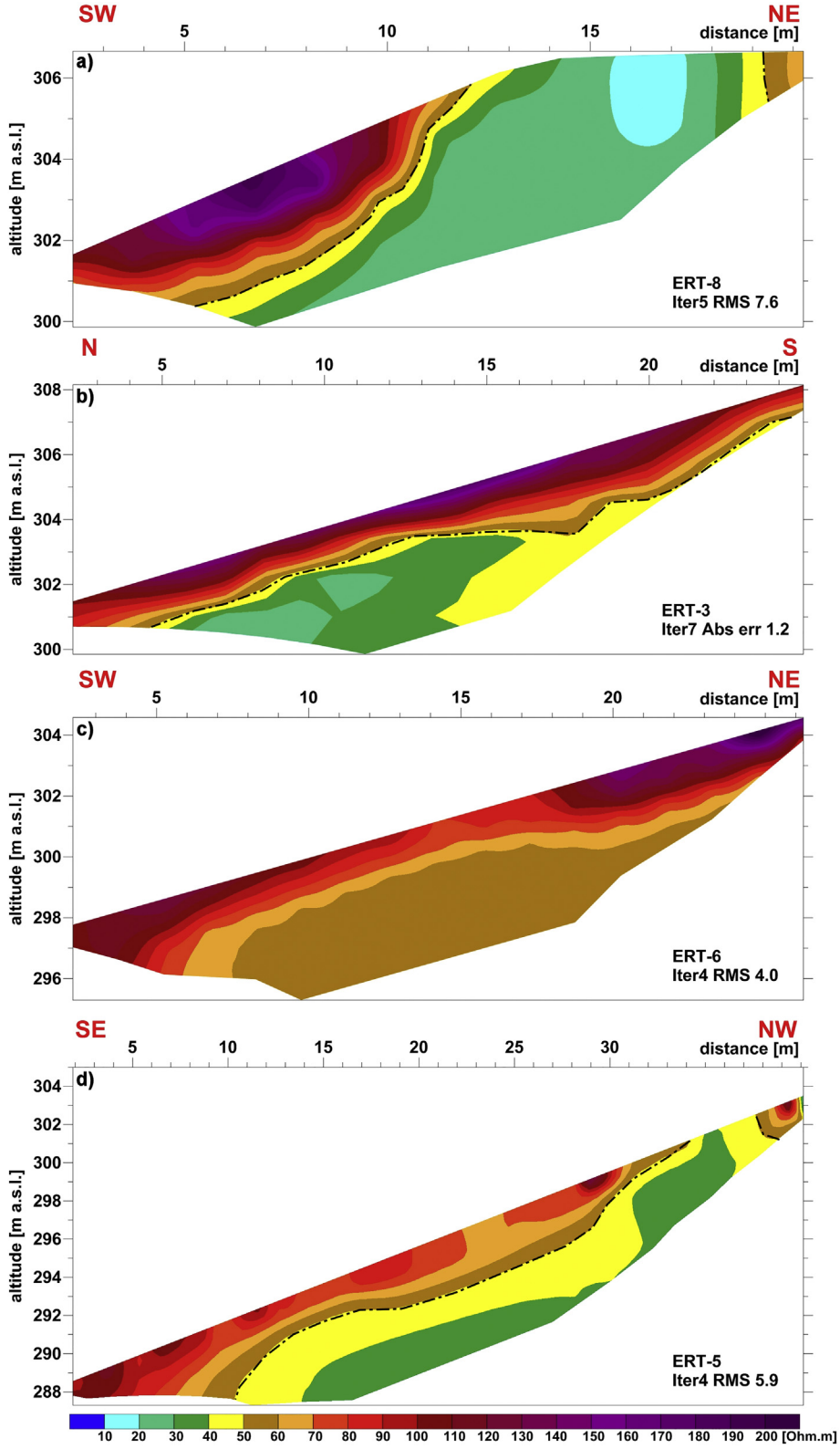

Fig. 9. ERT sections for selected traverses on the slopes of the dump. Dashed line is the interpreted roof of the urban waste. A – ERT-8. B – ERT-3. C – ERT-6. D – ERT-5.

where thermal phenomena had been noted (Fig. 3). On EM-1 (Fig. 10A), the apparent conductivity changes in the range 10–50 mS/m for VD = 1 m and 4–35 mS/m for VD = 0.5 m. The values determined for VD = 1.0 m, the deeper range, are 10–15 mS/m higher than for VD = 0.5 m on average. This can be explained by a decrease in coal-waste humidity near the surface. At 90 m from the western end of the traverse, the apparent conductivity gradually increases. The highest values for both configurations are seen between 90 and 210 m where the traverse crosses the roof of the dump. On the south-western slope, the conductivity decreases below 20 mS/m for VD = 1.0 m and 10 mS/

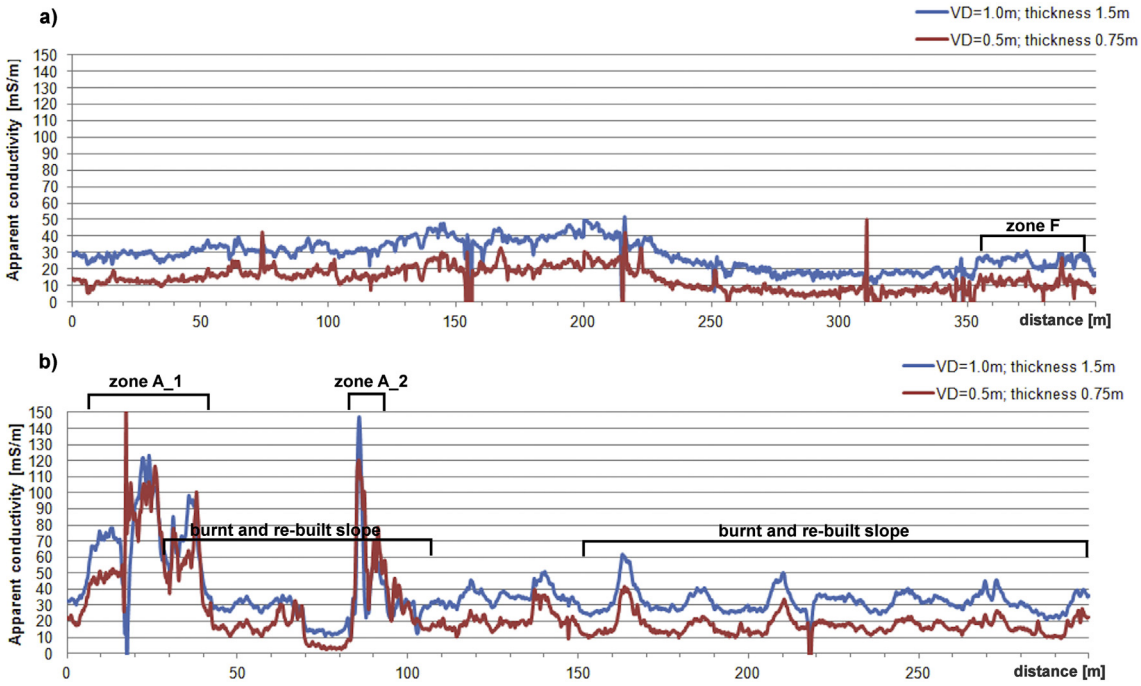

Fig. 10. Results of electromagnetic surveys of the dump. A – South-western slope. B – Northern slope.

m for VD = 0.5 m. Finally, at 350 m where short-lived thermal activity has been documented (zone F; Ciesielczuk et al., 2013), conductivity slightly increases but does not reach the level measured on the dump roof. The results from EM-1 confirm those from ERT; material with high resistivity resides mainly on the slopes.

The EM-2 traverse on the northern slope starts on the western border of the larger active field (zone I-zone A; Fig. 3), passes through the area showing no effects of heating and through the smaller zone A and, after continuing through the inactive central part of the northern slope, ends at the ditch cut when fire was extinguished in 2008 (Ciesielczuk et al., 2013). For the entire northern slope, apparent conductivities range from 10 to 25 mS/m for VD = 0.5 m to 25–45 mS/m for VD = 1.0 m. On average, these values are ~10 mS/m higher than those for the south-western slope (Fig. 10B). In both areas of recent thermal activity (zone A), the values for both configurations increase up to 120 mS/m. Our results agree with those of Uchtmann et al. (2013). For the more active fire spot 2 (Fig. 10B), apparent conductivities are similar for both depths ranges.

The conductivity changes in areas of recent thermal activity reflect chemical transformations of both organic- and inorganic coal-waste material due to heating. Though the presence of conductive carbon was reported by Fabiańska et al. (2017) for several samples from the Wełnowiec dump, increased ionic conductivity is likely to be the key factor affecting the electrical conductivity of active zones. Self-heating temperatures > 200 °C, and oxygen deficiency favor pyrolysis of kerogen in coal waste, the main products of which are water and bitumen composed of lighter organic compounds (m.w. < 500 Da; Misz-Kennan and Fabiańska, 2011). Active hot spots on dump surfaces are usually saturated with these substances. Typically, these moist areas are first indicators of heating below. Steam plumes from cracks and vents commonly encrusted with blooming minerals are further indicators (Fabiańska et al., 2013). Even when thermal activity wanes, these places retain some humidity promoting vegetation growth, despite the low soil quality (Abakumov and Frouz, 2013; Ciesielczuk et al., 2015a).

The enhanced ionic conductivity of water, commonly noted in areas of coal-waste storage, reflects increased contents of, e.g., SO_4, Cl, Na, Ca, Mg, Fe, Mn (Szczepańska-Plewa and Zdechlik, 2011). During self-heating, raised temperatures and increasing fragmentation promote dissolution of the mineral fraction in the waste, and acid drainage (Gorova et al., 2015). Water-soluble minerals formed during heating affect the mineralization of pore water. Sulphate- and sulphite ions derive from sulphur oxides formed from sulphides (mostly pyrite), carbonate- and bicarbonate ions from dissolved carbon dioxide and nitrite- and nitrate ions from nitrogen oxides (NO_x); with the latter, nitrogen-recycling bacteria living on coal waste may be involved (Hu et al., 2000; Frouz et al., 2014; Mahmmod, 2016). The presence of these ions in dump waters has been well documented (e.g., Mele et al., 1982; National Research Council, 1990; Mahmmod, 2016; Ciesielczuk et al., 2014a). Thus, the increased electrical conductivity of self-heating coal waste is due to ions produced by the heating and dissolved in pyrolytical water. An additional contributing factor may be enhanced microbiological activity (e.g., Atekwana and Atekwana, 2010).

Small increases in conductivity may also characterize areas of short-lived activity (zone F). However, amplitudes are lower than those due to variations in thickness of the dump rehabilitation layer, making unequivocal identification difficult. Increased conductivities in these areas may be due to heating-induced fragmentation of waste material.

Evident variations in the magnetic in-phase component of the EM field were not seen in either active- or burnt areas. The absence of magnetic minerals may reflect early pyrite decomposition due to weathering before any heating occurred, or to near-surface low temperatures inhibiting pyrite alteration later.

4. Conclusions

Applied geophysical methods reveal the internal structure of the Wełnowiec dump by distinguishing between municipal waste and its rehabilitated cover. The flat top of the dump, where the rehabilitation layers should be least distorted, was expected to reveal the planned structure of the rehabilitation layer. However, high-resolution ERT measurements reveal up to 26 m of municipal waste covered by the irregularly distributed material of varying thickness and composition instead of a designed 2.2-m-thick multi-barrier system. Though the thickness of coal waste in the barrier system was planned to be 0.9 m, the rehabilitation layer with a thickness of 1–8 m locally consists mainly of coal waste. Adjacent traverses indicate that the thickness of

the rehabilitation layer is markedly variable.

Heating and combustion started in the Wełnowiec dump because all three prerequisite conditions existed, namely, oxygen access, reactive coaly material and the possibility for heat accumulation; the lack of one or other rendered parts of the dump thermally passive. Where the volume of coal waste used in rehabilitation was much greater than planned, as on the northern slope of the dump, burning could spread for many years and require professional fire-fighting to stop it. Where, e.g., on the upper part of the south-western slope, the volume is only just sufficient, small hot spots (< ~20 m in diameter) appeared and waned spontaneously over a few years. Where the volume of coal waste is not adequate for thermal activity, e.g., where the rehabilitation layer is < 2.5 m in the central part of the northern slope, no thermal activity was seen either on the ground or in ERT sections. On the other hand, at the top of the dump where ~8 m of rehabilitation layer was proved, and ~5 m at the northern part of the eastern slope, thermal activity never started; limited oxygen access is the probable reason. Coal contents > 5% and a coal-waste layer thickness > 4 m appear to be minimum prerequisites for unpacked coal waste to self-heat in the Wełnowiec dump.

Reconstruction of the original architecture of the northern slope, the most active, is impossible due to partial rebuilding. For the other steep (≥ 20°) slopes, as the rehabilitation layer is thicker at their bases, it is conceivable that the architecture of any original barrier was destroyed by gravitational processes such as soil creep, interlayer slip, mass flow or landslides. Nevertheless, though the thickness of the coal waste is about 4–5 m, no heating started there. In the upper part of the eastern slope, the rehabilitation layer is discontinuous within 5–6 m from the top. The most probable reason was the rehabilitation layer creep or interlayer slip which by causing the observed fracturing in the upper parts of the slope facilitated oxygen circulation. Despite the fact that the break was not detected geophysically, the petrographic results suggest the relocation of the examined material. Enhanced air flow and water access in combination with sufficient coal-waste thickness promoted the thermal activity of the Wełnowiec waste dump.

Despite the complex structure of the rehabilitation layer and its relatively low organic carbon content, changes in conductivity in the areas of current heating in the dump are analogous to those observed in thermally-active coal fields. Active burning was clearly detected by EM. Distinct increases in conductivity identify thermally-active areas, even areas of waning activity; observed conductivities are more than double the maximum values recorded elsewhere in the dump.

Thermal activity detected by geophysical methods is also broadly reflected in changes in chemical composition, organic petrography, and geochemistry. Self-heating significantly changes the chemistry of the waste by modifying its mineral composition and triggering element migration. Minerals stable at low temperature rebuilt their structures, usually release moisture, or disintegrate. Initial-, active-, overburnt- and short-lived zones of thermal activity differ in their mineralogy and chemistry. Quartz, clay minerals, chlorite, micas, feldspars, and coal are ubiquitous in initial- and short-lived zones, present in lesser amounts in the active zone and absent in the overburnt zone. Phases such as celsian, anorthite, cordierite, mullite, olivine, augite, spinel group, gypsum, sal ammoniac, and glass, sparse in initial- and short-lived zones, are common in the active- and the overburnt zones. Minerals such as calcite, zircon, anatase, lead, iron, chalcopyrite and ZnS occurring in trace amount significantly influence chemical compositions. Bitumen is enriched with pyrolysate in the most thermally-active zones. In overburnt zones, it was destroyed by open fire.

In chemical terms, Si, Ti, Al, K, Sb, In and Sc are significant in the initial- and short-lived zones, and Fe, Mn, Mg, Ca, P, Sr, Ba, Se, Ce, Pr, Nd, Sn, Te and I in active- and overburnt zones. S, Cl, Zn, and Pb feature only in thermally-active zones. V, Cr, Co, Rb, and Ge show no correlation with thermal activity.

Though the mineral- petrographic- and chemical compositions of burnt- and initial-zone waste are very different, burnt- and unburnt waste are not unambiguously distinguishable by their conductivities. In the Wełnowiec dump, changes in electrical conductivity due to self-ignition are masked by other factors such as changes in thickness of the rehabilitation layer; change in conductivity due to variation in rehabilitation layer thickness is greater than that due to burnt waste. The inability of the applied geophysical methods to detect changes in coal waste caused by self-heating, after the process had ceased was unexpected.

Our results strongly suggest that the use of coal waste as a remediation layer covering waste dumps should be prohibited. Coal waste is simply too prone to unpredictable self-heating and self-ignition with the potential environmental consequences that follow. If coal waste is used the application should be in conjunction with properly planned spacers and barriers.

Acknowledgments

The authors would like to thank Prof. Janusz Janeczek (Faculty of Earth Sciences, University of Silesia) who drew our attention to the problem and encouraged our studies. Dr. Pádhraig Kennan (University College Dublin, Ireland) is thanked for language correction. This work was financially supported by NCN grant No. 2011/01/B/ST10/07588.

References

Abakumov, E., Frouz, J., 2013. Humus accumulation and humification during soil development in post-mining soil. In: Frouz, J. (Ed.), Soil Biota and Ecosystem Development in Post Mining Sites. CRC Press, pp. 19–37.

Atekwana, E., Atekwana, E., 2010. Geophysical signatures of microbial activity at hydrocarbon contaminated sites: a review. Surv. Geophys. 31, 247–283.

Atlas Geologiczno-Inżynierski Aglomeracji Katowickiej (Geo-engineering Atlas of Katowice Agglomeration). http://bazadata.pgi.gov.pl/data/atlasy_gi_otwory, Accessed date: December 2018.

Atomic Absorption Spectrometry, 2000. Methods Manual. Unicam Limited (Registration No.441506).

Brooks, K., Svanas, N., Glasser, D., 1988. Evaluating the risk of spontaneous combustion in coal stockpiles. Fuel 67 (5), 651–656.

Ciesielczuk, J., Janeczek, J., Cebulak, S., 2013. Przebieg i przyczyny endogenicznego pożaru węgla kamiennego na zredukowanym składowisku odpadów komunalnych w Katowicach (*The cause and progress of the endogenous coal fire in the remediated landfill in the city of Katowice*). Prz. Geol. 61 (12), 764–772 (in Polish).

Ciesielczuk, J., Kruszewski, Ł., Fabiańska, M.J., Misz-Kennan, M., Lewińska-Preis, L., Kita, A., 2014a. Composition of water located in the coal waste dumps in Lower Silesia, Poland. Min. Spec. Pap. 42, 46.

Ciesielczuk, J., Misz-Kennan, M., Hower, J.C., Fabiańska, M.J., 2014b. Mineralogy and geochemistry of coal wastes from the Starzykowiec coal-waste dump (Upper Silesia, Poland). Int. J. Coal Geol. 127, 42–55.

Ciesielczuk, J., Czylok, A., Fabiańska, M.J., Misz-Kennan, M., 2015a. Plant occurrence on burning coal waste – a case study from the Katowice-Wełnowiec dump, Poland. Environ. Socio-econ. Stud. 3 (2), 1–10.

Ciesielczuk, J., Kruszewski, Ł., Majka, J., 2015b. Comparative mineralogical study of thermally-altered coal-dump waste, natural rocks and the products of laboratory heating experiments. Int. J. Coal Geol. 139, 114–141.

Creelman, R.A., Ward, C.R., Shumacher, G., Juniper, L., 2013. Relation between coal mineral matter and deposit mineralogy Pulverised Fuel Furnaces. Energy Fuel 27, 5714–5724.

Dai, S., Ren, D., Hou, X., Shao, L., 2003. Geochemical and mineralogical anomalies of the late Permian coal in the Zhijin coalfield of southwest China and their volcanic origin. Int. J. Coal Geol. 55, 117–138.

Dai, S., Li, D., Ren, D., Tang, Y., Shao, L., Song, H., 2004. Geochemistry of the late Permian No. 30 coal seam, Zhijin Coalfield of Southwest China: influence of a siliceous low-temperature hydrothermal fluid. Appl. Geochem. 19, 1315–1330.

Dai, S., Ren, D., Tang, Y., Yue, M., Hao, L., 2005. Concentration and distribution of elements in Late Permian coals from western Guizhou Province, China. Int. J. Coal Geol. 61, 119–137.

Dai, S., Zou, J., Jiang, Y., Ward, C.R., Wang, X., Li, T., Xue, W., Liu, S., Tian, H., Sun, X., Zhou, D., 2012. Mineralogical and geochemical compositions of the Pennsylvanian coal in the Adaohai Mine, Daqingshan Coalfield, Inner Mongolia, China: Modes of occurrence and origin of diaspore, gorceixite, and ammonian illite. Int. J. Coal Geol. 94, 250–270.

Donelly, L.J., Bell, F.G., 2011. Geotechnical and environmental problems. In: Stracher, G.B., Prakash, A., Sokol, E.V. (Eds.), Coal and Peat Fires: A Global Perspective. 1. Elsevier, Amsterdam, pp. 84–99.

Duba, A., 1977. Electrical conductivity of coal and coal char. Fuel 56, 441–443.

Duba, A., 1983. Electrical conductivity of Colorado oil shale to 900 °C. Fuel 62, 966–972.

Dulewski, J., Madej, B., Uzarowicz, R., 2010. Zagrożenie procesami termicznymi obiektów zagospodarowania odpadów z górnictwa węgla kamiennego (*The hazards of heating processes in the facilities of coal mining waste management*). Gospodarka

Surowcami Mineralnymi 26 (3), 125–142 (in Polish).
Edjabou, M.E., Astrup, T.F., Scheutz, Ch., 2016. Composition of municipal solid waste in Denmark. Technical University of Denmark, pp. 69.
Fabiańska, M.J., Ćmiel, S.R., Misz-Kennan, M., 2013. Biomarkers and aromatic hydrocarbons in bituminous coals of Upper Silesian Coal Basin: Example from 405 coal seam of the Zaleskie Beds (Poland). Int. J. Coal Geol. 107, 96–111.
Fabiańska, M.J., Misz-Kennan, M., Ciesielczuk, J., Pierwoła, J., Nitecka, N., Brzoznowski, J., 2017. Thermal history of coal wastes reflected in their organic geochemistry and petrography; the case study: The Katowice-Wełnowiec dump, Poland. Int. J. Coal Geol. 184, 11–26.
Finkelman, R.B., 1993. Trace and minor elements in coal. In: Engel, M.H., Macko, S.A. (Eds.), Organic Geochemistry. Plenum, New York, pp. 593–607 (Chap. 28).
Flötzkarte des Oberschlesischen Steinkohlenbeckens, 1903. No 26 Sect. Kattowitz. http://maps.mapywig.org/m/German_maps/series/010K_Floetzkarte_Oberschlesien/Floetzkarte_des_Oberschlesischen_S._No_26_Sect.Kattowitz.jpg, Accessed date: 12 December 2017.
Frouz, J., Elhottava, D., Baldrian, P., Chronakowa, A., Likesova, A., Novakova, A., Kristufek, V., 2014. Soil microflora development in post-mining sites. In: Frouz, J. (Ed.), Soil Biota and Ecosystem Development in Post Mining Sites. CRC Press, pp. 104–131 (Chap. 7).
Gorova, A., Pavlychenko, A., Kulyna, S., 2015. Environmental aspects of waste management on coal mining enterprises. In: Pivnyak, G., Bondarenko, V., Kovalevska, I. (Eds.), New Developments in Mining Engineering 2015: Theoretical and Practical Solutions of Mineral Resources Mining. CRC Press, Tylor & Francis Group ((600 pp), ISBN: 1315648776, 9781315648774).
Heffern, E.L., Coates, D.A., 2004. Geologic history of natural coal-bed fires, Powder River basin, USA. Int. J. Coal Geol. 59, 25–47.
Hu, Y., Naito, S., Kobayashi, N., Hasatani, M., 2000. CO_2, NOx and SO_2 emissions from the combustion of coal with high oxygen concentration gases. Fuel 79, 1925–1932.
ISO 7404-3, 2009. Methods for the petrographic analysis of coals - Part 3: Method of determining maceral group composition. International Organization for Standardization, Geneva, Switzerland (7 pp).
ISO 7404-5, 2009. Methods for the petrographic analysis of coals - Part 5: Method of determining microscopically the reflectance of vitrinite. International Organization for Standardization, Geneva, Switzerland (11 pp).
Karaoulis, M., Revil, A., Mao, D., 2014. Localization of a coal seam fire using combined self-potential and resistivity data. Int. J. Coal Geol. 128–129, 109–118.
Kaymakçi, E., Didari, V., 2002. Relations between coal properties and spontaneous combustion parameters. Turk. J. Eng. Environ. Sci. 26 (1), 59–64.
King, A., 1987. Cindered coal detection using transient electromagnetic methods. Geoexploration 24, 367–379.
Klejnowska, H., 1996. Projekt budowlany: zagospodarowanie zielenią parkową terenu byłego składowiska odpadów komunalnych w Katowicach przy ul. Ludwika-Leopolda. I i II etap (uszczelnienie i odgazowanie sektora "C"). *(Engineering project: development of park green of the former municipal waste landfill in Katowice at Louis-Leopold Street. The first and second stage (sealing and degassing of the "C" sector))*. Biuro Usług Techn. EKOTEST s.c., Gliwice (32 pp). (in Polish).
Kotyrba, A., Grądziel, M., Gogola, K., 2012. Zastosowanie metody elektrooporowej w badaniach stanu termicznego zwałowisk odpadów powęglowych (*Application of the electrical resistance method in investigations of the thermal state of coal waste dumps*). Przegląd Górniczy 4, 53–61 (in Polish).
Kříbek, B., Sýkorová, I., Veselovský, F., Laufek, F., Malec, J., Knésl, I., Majer, V., 2017. Trace element geochemistry of self-burning and weathering of a mineralized coal waste dump: the Novátor mine, Czech Republic. Int. J. Coal Geol. 173, 158–175.
Krishnaswamy, S., Agarwal, P.K., Gunn, R.D., 1996a. Low-temperature oxidation of coal. 3. Modelling spontaneous combustion in coal stockpiles. Fuel 75 (3), 353–362.
Krishnaswamy, S., Bhat, S., Gunn, R.D., Agarwal, P.K., 1996b. Low-temperature oxidation of coal. 1. Single-particle reaction – diffusion model. Fuel 75 (3), 333–343.
Kruszewski, Ł., 2013. Supergene sulphate minerals from the burning coal mining dumps in the Upper Silesian Coal Basin, South Poland. Int. J. Coal Geol. 105, 91–109.
Kruszewski, Ł., Ciesielczuk, J., Misz-Kennan, M., Fabiańska, M., 2014. Chemical composition of glasses and associating mineral species in various pyrometamorphic rocks from coal-mining dumps of the Lower Silesia. Min. Spec. Pap. 42, 70–71.
Lyman, R.M., Volkmer, J.E., 2001. Pyrophoricity (spontaneous combustion) of Powder River Basin coals – consideration for coalbed methan development. Coal report CR 01-1. http://www.wsgs.wyo.gov/products/wsgs-2001-cr-01.pdf
Mahmmod, F.N., 2016. Nitrate in coal waste rock dumps, Elk Valley, British Columbia, Canada. College of Graduate Studies and Research, Department of Geological Sciences University of Saskatchewan, Saskatoon (59 pp, MSc Thesis).
Martínez, M., Márquez, G., Alejandre, F.J., Del Río, J.J., Hurtado, A., 2009. Geochemical study of products associated with spontaneous oxidation of coal in the Cerro Pelado Formation, Venezuela. J. South Am. Earth Sci. 27, 211–218.
Mele, L.M., Prodan, P.F., Schubert, J.P., 1982. Characterization of runoff water from coal-waste disposal sites in southwestern Illinois. Int. J. Mine Water 1, 1–14.
Meyer, U., Gundelach, V., Vasterlin, M., Lambrecht, A., Rueter, H., Lindner, H., 2009. Geophysical methods for coal fire detection and monitoring. In: American Geophysical Union, Fall Meeting 2009, (abstract NS44A-03, 1 pp).
Miezah, K., Obiri-Danso, K., Kádár, Z., Fei-Baffoe, B., Mensah, M.Y., 2015. Municipal solid waste characterization and quantification as a measure towards effective waste management in Ghana. Waste Manag. 46, 15–27.
Misz-Kennan, M., Fabiańska, M.J., 2011. Application of organic petrology and geochemistry to coal waste studies. Int. J. Coal Geol. 88, 1–23.
Nadłonek, W., Cabała, J., 2016. Potentially toxic elements in soils and plants on a reclaimed coal-waste dump in southern Poland (preliminary study). Acta Geodyn. Geomater. 13 (183), 271–279.
National Research Council, 1990. Groundwater quality: effects of coal surface mining. In: Surface Coal Mining Effects on Ground Water Recharge. National Academy Press, Washington USA, pp. 142–149.
Parafiniuk, J., Kruszewski, Ł., 2009. Ammonium minerals from burning coal-dumps of the Upper Silesian Coal Basin (Poland). Geol. Q. 53, 33–47.
Parafiniuk, J., Kruszewski, Ł., 2010. Minerals of the ammonioalunite-ammoniojarosite series formed on a burning coal dump at Czerwionka, Upper Silesian Coal Basin, Poland. Min. Mag. 74, 731–745.
Pone, J.D.N., Hein, K.A.A., Stracher, G.B., Annegarn, H.J., Finkelman, R.B., Blake, D.R., McCormack, J.K., Schroeder, P., 2007. The spontaneous combustion of coal and its by-products in the Witbank and Sasolburg coalfields of South Africa. Int. J. Coal Geol. 72, 124–140.
Prakash, A., Gens, R., Prasad, S., Raju, A., Gupta, R.P., 2013. Jharia coalfield fires, India. In: Stracher, G.B., Prakash, A., Sokol, E.V. (Eds.), Coal and Peat Fires: A Global Perspective. vol. 2. Elsevier, Amsterdam, pp. 154–176.
Qing, S., Wang, Y., 2010. Application of electric and magnetic approaches in coalfield fire detection in Xinjiang. In: Latest Developments in Coal Fire Research. Bridging the Science, Economics, and Politics of a Global Disaster. Proc. of 2nd International Conference on Coal Fire Research, pp. 398–399.
Revil, A., Karaoulis, M., Srivastava, S., Byrdina, S., 2013. Thermoelectric self-potential and resistivity data localize the burning front of underground coal fires. Geophysics 78 (5), B259–B273.
Ribeiro, J., Ferreira Da Silva, E., Li, Z., Ward, C., Flores, D., 2010. Petrographic, mineralogical and geochemical characterization of the Serrinha coal waste pile (Douro Coalfield, Portugal) and the potential environmental impacts on soil, sediments and surface waters. Int. J. Coal Geol. 83, 456–466.
Ribeiro, J., Moura, R., Flores, D., Lopes, D.B., Gouveia, C., Mendonça, S., Frazão, O., 2013. The Douro coalfield fires of Portugal. In: Stracher, G.B., Prakash, A., Sokol, E.V. (Eds.), Coal and Peat Fires: A Global Perspective. vol. 2. Elsevier, Amsterdam, pp. 314–337.
Ribeiro, J., Suarez-Ruiz, I., Ward, C.R., Flores, D., 2016. Petrography and mineralogy of self-burning coal waste dumps from anthracite mining in the El Bierzo Coalfield (NW Spain). Int. J. Coal Geol. 154–155, 92–106.
Sanei, H., Carrie, J., Goodarzi, F., 2013. Canadian coal fires. In: Stracher, G.B., Prakash, A., Sokol, E.V. (Eds.), Coal and Peat Fires: A Global Perspective. vol. 2. Elsevier, Amsterdam, pp. 26–37.
Sant'Ovaia, H., Ribeiro, J., Correa-Ribeiro, H., Gomes, C., Li, Z., Ward, C., Flores, D., 2010. An integral study of mineralogy and magnetic parameters of coal waste pile materials in combustion from Douro Coal Field (Portugal): first results of a case study. In: Latest Developments in Coal Fire Research. Bridging the Science, Economics, and Politics of a Global Disaster. Proc of 2nd International Conference on Coal Fire Research, pp. 408–409.
Sawicki, T., 2004. Samozapalenie węgla w zwale jako przyczyna pożarów (*Spontaneous combustion in stock piles as the cause of fire*). Karbo 1, 56–59 (in Polish).
Schaumann, G., Siemon, B., Changchun, Y., 2008. Geophysical investigation of Wuda coal mining area, inner Mongolia: electromagnetics and magnetics for coal fire detection. In: *Spontaneous coal seam fires: Mitigating a global disaster. International Research for sustainable control and management.* ERSEC Ecological Book Series – 4. Tsinghua University Press and Springer Verlag, Beijing (18 pp).
Schön, J.H., 2015. Physical Properties of Rocks: Fundamentals and Principles of Petrophysics. Elsevier, Amsterdam (497 pp).
Shao, Z., Wang, D., Wang, Y., Zhong, X., Tang, X., Xi, D., 2016. Electrical resistivity of coal-bearing rocks under high temperature and the detection of coal fires using electrical resistance tomography. Geophys. J. Int. 204 (2), 1316–1331.
Skarżyńska, K.M., 1995. Reuse of coal mining wastes in civil engineering. Part 1: properties of minestone. Waste Manag. 15 (1), 3–42.
Sokol, E.V., Maksimova, N.V., Nigmatulina, E.N., Sharygin, V.V., Kalugin, V.M., 2005. Combustion metamorphism. Publishing House of the SB RAS, Novosibirsk (312 pp. in Russian).
Soto, M.D., Urbani, F., 2015. The "volcanoes" of Midwestern Venezuela. In: Stracher, G.B., Prakash, A., Sokol, E.V. (Eds.), Coal and Peat Fires: A Global Perspective. vol. 3. Elsevier, Amsterdam, pp. 610–632.
Stracher, G.B., Prakash, A., Sokol, E.V. (Eds.), 2011. Coal and Peat Fires: A Global Perspective. vol. 1 Elsevier, Amsterdam (357 pp).
Stracher, G.B., Prakash, A., Sokol, E.V. (Eds.), 2013. Coal and Peat Fires: A Global Perspective. vol. 2 Elsevier, Amsterdam (786 pp).
Stracher, G.B., Prakash, A., Sokol, E.V. (Eds.), 2015. Coal and Peat Fires: A Global Perspective. vol. 3 Elsevier, Amsterdam (554 pp).
Suggate, R.P., 1982. Low rank sequences and scales of organic metamorphism. J. Pet. Geol. 4 (4), 377–392.
Sýkorová, I., Kříbek, B., Havelcová, M., Machovič, V., Laufek, F., Veselovský, F., Špaldoňová, A., Lapčák, L., Knésl, I., Matysová, P., Majer, V., 2018. Hydrocarbon condensates and argillites in the Eliška Mine burnt coal waste heap of the Žacléř coal district (Czech Republic): Products of high- and low-temperature stages of self-ignition. Int. J. Coal Geol. 190, 146–165.
Szczepańska-Plewa, J., Zdechlik, R., 2011. Badania hydrogeologiczne. In: Marcak, H., Tomecka-Suchoń, S., Zdechlik, R. (Eds.), Geofizyczne i hydrogeologiczne badania zanieczyszczeń środowiska wodno-gruntowego w otoczeniu składowisk odpadów górniczych (*Geophysical and Hydrogeological Studies on Pollution of Soil-Water Environment in the Surroundings of Mine Waste Deposits*). Oficyna Drukarska – Jacek Chmielewski, Warszawa (33 pp. in Polish).
Uchtmann, S., Brenner, O., Swoboda, U., Elsen, R., Orlowsky, D., 2013. Geophysical Investigation of a Burning Dump in Estonia – A Case Study. Near Surface Geoscience 2013 – 19th European Meeting of Environmental and Engineering Geophysics Bochum, Germany, 9–11 September 2013, Tu S2b 11.
Ward, C.R., 2002. Analysis and significance of mineral matter in coal seams. Int. J. Coal Geol. 50, 135–168.

Ward, C.R., 2016. Analysis, origin and significance of mineral matter in coal: an updated review. Int. J. Coal Geol. 165, 1–27.
Ward, C.R., Spears, D.A., Booth, C.A., Staton, I., Gurba, L.W., 1999. Mineral matter and trace elements in coals of the Gunnedah Basin, New South Wales, Australia. Int. J. Coal Geol. 40, 281–308.
Zapał, A., Ratomski, J., 2007. Geotechniczna ocena przydatności odpadów kopalnianych w hydrotechnicznym budownictwie ziemnym (*Geotechnical assessment of suitability of mine wastes in hydrotechnical earth structures*). Czasopismo Techniczne. Wydawnictwo Politechniki Krakowskiej, pp. 227–237 (in Polish).